

AERODYNAMIC MODELLING OF AVIAN-INSPIRED ASYMMETRIC WING TIP MORPHING MECHANISMS

By

OBINAJU, PRECIOUS OBIANUJU

MSc Aerial Robotics Dissertation



Department of Engineering Mathematics

UNIVERSITY OF BRISTOL

An MSc dissertation submitted to the University of Bristol

in accordance with the requirements of the degree of

MASTER OF SCIENCE IN AERIAL ROBOTICS in the

Faculty of Engineering.

September 19, 2023

Declaration of own work

I declare that the work in this MSc dissertation was carried out in accordance with the requirements of the University's Regulations and Code of Practice for Research Degree Programmes and that it has not been submitted for any other academic award. Except where indicated by specific reference in the text, the work is the candidate's own work. Work done in collaboration with, or with the assistance of, others, is indicated as such. Any views expressed in the dissertation are those of the author.

Obinaju, Precious O.

5th September, 2023

Acknowledgement

I would like to thank God for his mercy and grace that accompanied me throughout the duration of this MSc.

Special Thanks to my supervisor and programme coordinator: Professor Tom Richardson for his assistance and support during this research. I want to express my deep appreciation to my wonderful Parents Prof. and Prof.(Mrs) J.N. Obinaju for their financial and moral support during my master's programme.

I also want to appreciate all the academics and technical staff at the University of Bristol that aided in making this research a success. To my family and friends I extend my sincere gratitude for the moral support that was made readily available to me throughout the course of this degree.

Abstract

This project attempted to solve the problem of uncertainty regarding the variation in control authority at different degrees of actuation of asymmetric wing tip twist and sweep at low speeds and high angles of attack. It aimed to achieve this by modelling and evaluating a bio-inspired wing using both mechanisms for flight control in fixed wing UAVs. This research focused on the aerodynamic characteristics of the wing excluding the effects of the fuselage and tail section of the UAV.

The objectives of this research were achieved by designing a wing model inspired by Ajanic's LisHawk. This wing model was analysed using Strip Theory and Ring Vortex Lattice Method available in the Flow 5 analysis Tool. These results were compared against results obtained through wind tunnel experiments. A second iteration of this analysis was done on a wing model inspired by the model tested by Groves-Raines 2022 aimed at proffering a means of realistically actuating these mechanisms.

The results obtained from these analyses indicate that asymmetric wing tip sweep and twist can be used to generate large changes in the aerodynamic moments and lateral stability of the model at high angles of attack. Results also indicate that asymmetric wing tip twist has large effects on control authority available during flight control. These results suggest that asymmetric wing tip sweep and twist can be used as flight control mechanisms that improve the agility and maneuverability of fixed wing UAVs at low speeds and high angles of attack. Utilising this mechanisms can increase the performance of fixed wing UAVs in applications that involve clustered environments and turbulence such as urban environments.

Number of words in the dissertation: 9062 words.

Contents

	Page
1 Introduction	8
1.1 Background of the Study	8
1.2 Problem Statement	9
1.3 Aim	9
1.4 Core Objectives	9
1.5 Stretch Objective	10
1.6 Research Scope and Limitations	10
1.7 Project Management	10
2 Literature Review	13
3 Research Methodology	18
3.1 Tapered Wing Tip	18
3.2 Feather-like Structured Wing Tip	29
4 Results	35
4.1 Tapered Wing Tip Aerodynamic Model Data	35
4.2 Comparison of Results of Feather-like Structured Wing Tip Model Against Tapered Wing Tip Model	45
5 Discussion and Conclusion	48
5.1 Research Summary	48
5.2 Research Limitations	49
5.3 Research Applications and Impact	49
References	56

List of Tables

1.1	Risk scoring scheme	11
1.2	Compiled Risk Register for Research	12
3.1	Summary of Wing Dimensions.	18
3.2	Summary of Wing Masses.	27
3.3	Summary of Wing Dimensions for Feather-like Structures.	31

List of Figures

1.1	Proposed Timeline For The Research	11
2.1	Illustration of Conventional and Avian Flight Controls (Harvey et al, 2022) [1]	14
2.2	Simplified Illustrations of the Different UAV Implementations of Bio-Inspired Wing Sweep (Harvey et al, 2022) [1]	15
2.3	a. Drone illustrating asymmetric wrist-inspired wing sweep b. Drone illustrating asymmetric wing twist. (Ajanic et al, 2022)[6]	16
3.1	Wing Model Design Dimensions	19
3.2	Wing Tip Backward Sweep Dimensions	20
3.3	Wing Tip Forward Sweep Dimensions	22
3.4	Wing Tip Twist Dimensions	24
3.5	Flow 5 Wing Model for Feather-like Structured Wing Tip	25
3.6	Wing Tip Twist Dimensions	27
3.7	Wind Tunnel Setup with the Wing in Symmetrical Configuration	28
3.8	Wing Model Design for Feather-like Structured Wing Tip	29
3.9	Strip Theory Wing Representation	30
3.10	Flow 5 Wing Model for Feather-like Structured Wing Tip	34
4.1	Rolling Moment (Nm) vs. Angle of Attack ($^{\circ}$) for Varying Sweep Angles at 12m/s	35
4.2	Rolling Moment (Nm) vs. Angle of Attack ($^{\circ}$) for Varying Twists Angles at 12m/s	37
4.3	Lift Coefficient vs. Angle of Attack ($^{\circ}$) at 12m/s: Wind Tunnel Data vs Flow 5 Data	38
4.4	Drag Coefficient vs. Angle of Attack ($^{\circ}$): Wind Tunnel Data vs Flow 5 Model at 12m/s	40
4.5	Rolling Moment (Nm) vs. Angle of Attack ($^{\circ}$) for Varying Sweep Angles at 12m/s	41

4.6	Rolling Moment (Nm) vs. Angle of Attack ($^{\circ}$) for Varying Sweep and Twist Angles at 12m/s: Wind Tunnel Data Comparisons	42
4.7	Pitching Moment (Nm) vs. Angle of Attack ($^{\circ}$): Wind Tunnel Data vs Flow 5 Data at 12m/s	43
4.8	Yawing Moment (Nm) vs. Angle of Attack ($^{\circ}$) for Varying Twist Angles at 12m/s: Wind Tunnel Data vs Flow 5 Data	44
4.9	Data Comparison For Feather-Like Structured Wing Tip vs Tapered Wing Tip	47

1 Introduction

1.1 Background of the Study

Bio-inspiration for wing design has been the centre of much researches [1] as avian flight has been analysed to have multiple advantages in the aspect of control over current mechanisms in fixed wing UAVs such as better manoeuvrability through cluttered environments and the ability to withstand gusts during flight in urban air spaces. However, bio-inspired wing designs are difficult to model accurately as they present a number of parameters which are negligible in conventional wings. Attempts to model the aerodynamic characteristics of the wing usually require a significant number of assumptions thereby creating a gap between reality and the model. The uncertainty and complexity associated with the response of the aerodynamic surfaces in bio-inspired UAVs to control inputs present a challenge when trying to dynamically model the system. A different argument exists as well stating that biological systems are not solely optimised for flight as evolution of biological design prioritises other characteristics such as nutrition and reproduction over flight. Therefore identifying the key attributes of a biological system such as a bird's wing that can be directly applicable to drone design runs the risk of drafting unnecessary properties which results in added complexity of design.

Wing sweep and wing twist have been considered separately as mechanisms for flight control [2][3] and their individual effects analysed. Research has shown that asymmetric wing twist and sweep can be used for roll control. By observing both mechanism's uses in natural avian flight and benefits especially in adverse weather conditions, gust response and complex manoeuvres make it worth researching. A combination of both mechanisms have been found to be applicable in the dynamic change of the Goshawk wing which enables it to achieve aggressive flight in cluttered environments [4], [5]. By combining wing sweep with wing twist the aerodynamic properties of the wing could be modified for different flight conditions.

The combination of both wing sweep and twist in UAV design is a novel area of research that

has been explored by a few researchers to prove it's efficiency in reducing the turn radius in fixed wing flight[6].

1.2 Problem Statement

To validate the mass penalty and complexity in design associated with implementing these mechanisms against conventional designs a lot is yet to be discovered. This includes the variation in control authority at different degrees of actuation, low speeds and high angles of attack . This encapsulates the question being answered by this project. I have been fascinated by the degrees of freedom available in avian flight and therefore decided to pursue this as a project. I believe that the results from this project will aid in the research advancement and application of bio-inspired wing morphing as the level of uncertainty in the response generated by these mechanisms has posed a challenge in ascertaining the level of safety associated with the design.

1.3 Aim

The aim of this project is to model and evaluate a bio-inspired wing using wing tip sweep and twist as flight control mechanisms in fixed wing UAVs. It serves to provide information for further research on the optimal degrees of wing sweep and twist in flight control.

1.4 Core Objectives

1. Create baseline avian inspired wing and aerodynamic results influenced by [7], [8]
2. Model the aerodynamic characteristics of a dynamically bio-inspired wing with varying wing tip sweep and wing twist for selected angles of attack using Flow 5 analysis tool.
3. Conduct a series of wind tunnel experiments to measure the aerodynamic performance of the wing at varying air speeds, and degrees of actuation.
4. Revise avian wing model and design for realistic actuation.

1.5 Stretch Objective

1. Compare and contrast the performance of bio-inspired wing controls against conventional fixed wing ailerons in real world flight conditions.

1.6 Research Scope and Limitations

The scope of this research focuses on the aerodynamic characteristics of the wing excluding the effect of the fuselage and tail section of the UAV. It is important to know that this research model was not optimised for real life flight conditions and was conducted using a high camber aerofoil; therefore slight differences are to be expected if these results are to be implemented on an actual UAV. While this research primarily focused on the rolling moment generated by the bio-inspired control mechanisms, it also gave account of other moments generated by the wing models.

1.7 Project Management

To achieve the objectives of this project, project management played a critical role. Regular meetings and updates were scheduled with the supervisor of this research to discuss the progress and milestones achieved. Also the detailed timeline shown in Figure 1.1 proposed at the commencement of this project was consulted periodically to ensure that milestones were achieved within their stipulated time frames. Although the timeline was not followed strictly, it proved to be important in the time regulation of activities conducted during this research.

Furthermore, A risk register was compiled at the onset of this project as shown in Table 1.2 with risks, likelihoods and impacts weighted using the scoring scheme shown in Table 1.1. During the duration of this project the mitigations highlighted were employed to ensure reduced likelihoods and impacts of the identified risks.

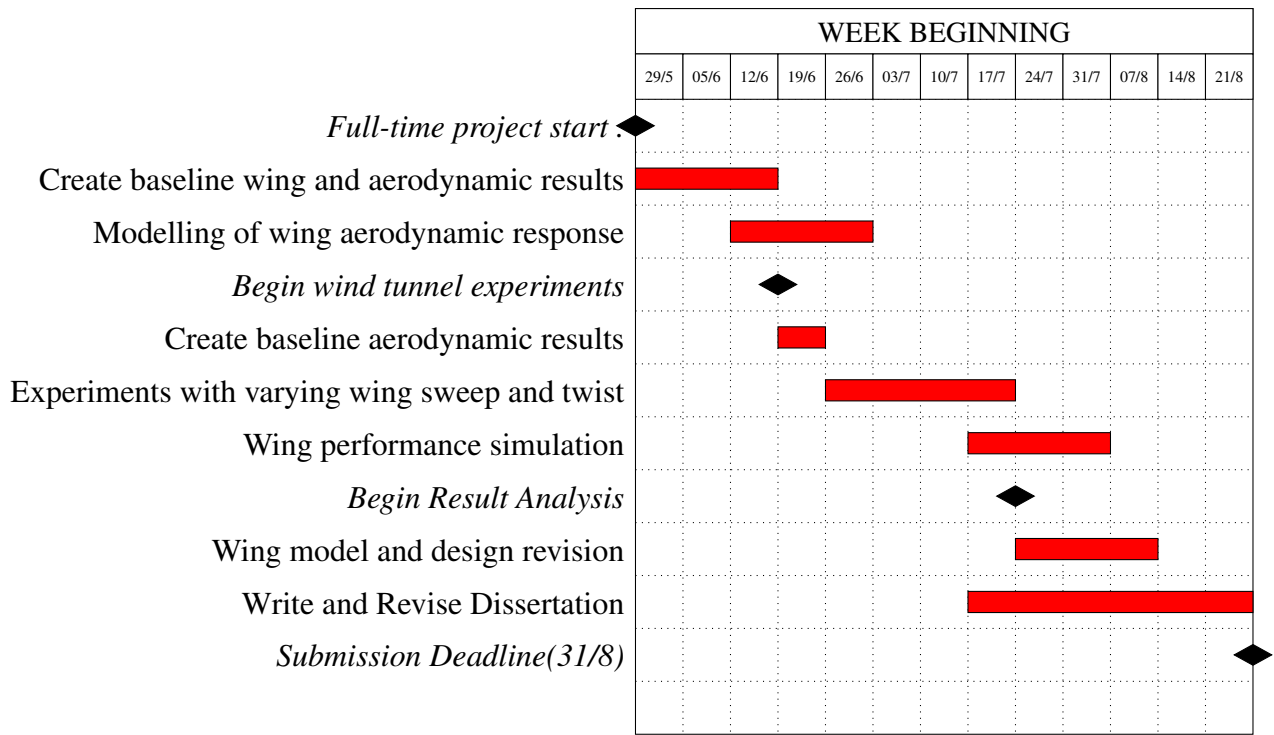


Figure 1.1: Proposed Timeline For The Research

Score	Likelihood	Impact
1	Very Unlikely to happen	Almost no disruption
2	Unlikely to happen	Some disruption
3	Likely to happen	Significant disruption
4	Very likely to happen	Total stoppage of project

Table 1.1: Risk scoring scheme

Risk	Mitigation	Likelihood(A)	Impact(B)	Risk Score(AB)
Unavailability of wind tunnels	Reserve the wind tunnels and load cells in advance. Design the wing to fit into two wind tunnels	2	3	6
Lack of time for design caused by material selection	Start early with design and simplify wing design	2	3	6
Experiment time overrun	Disregard stretched objectives	3	2	6
Complexity in simulating wing performance	Utilise a simpler model and build on model as results are obtained	2	2	4
Wing doesn't provide desired control authority	Document and learn from wing's response	2	1	2

Table 1.2: Compiled Risk Register for Research

2 Literature Review

Current fixed-wing UAVs use ailerons, elevators and rudders to manoeuvre in flight[9]–[11] as illustrated in Figure 2.1a. One of the issues often found with operating fixed-wing UAVs is its inability to deal with gust and high levels of turbulence which is characteristic of flight in complex environments at low altitudes such as urban air spaces[12]–[15]. Also multi-rotor drones although less aerodynamically and energetically efficient than fixed-wing drones are most commonly used for agile complex manoeuvres due to their ability to outperform conventional fixed wing UAVs in this regard. It has been observed that avian flight possesses a level of agility and manoeuvrability yet to be achieved by conventional fixed wing UAVs[16]. This ability allows birds to navigate through forests and crowded areas as well as perform evasive maneuvers to escape predators [17], [18]. This ability has been linked to bird's use of wing morphing techniques for flight control [19], [20]. This has inspired a lot of researchers to design mechanical systems aimed at mimicking natural flight.

Further studies of biological systems have shown that birds use muscular control to actuate their skeleton to realise a wide range of distinct wing shapes in flight as shown in Figure 2.1b [21] which in turn has effects on their flight control and stability allowing for complex manoeuvres[22][1][23][4]. Chin 2017 [16], in a study of the skeletal and muscle functions in birds highlights that natural selection has designed wings of birds to result in robust, versatile solutions for flight. This has led to a large volume of research focused on avian inspired wing morphing aimed at analysing its benefits, performance as well as comparing these against conventional fixed-wing controls while seeking to improve these designs. Wing morphing mechanisms can be classified into sweep, dihedral, twist, camber and alula [1]. Two morphing mechanisms will be focused on in this project; wing sweep and wing twist.

Wing sweep has been considered in many regards ranging from shoulder inspired morphing to wrist-inspired morphing designs and has been implemented successfully on many UAVs as summarised in Figure 2.2[1]. This morphing mechanism has been identified to reduce the lift slope,

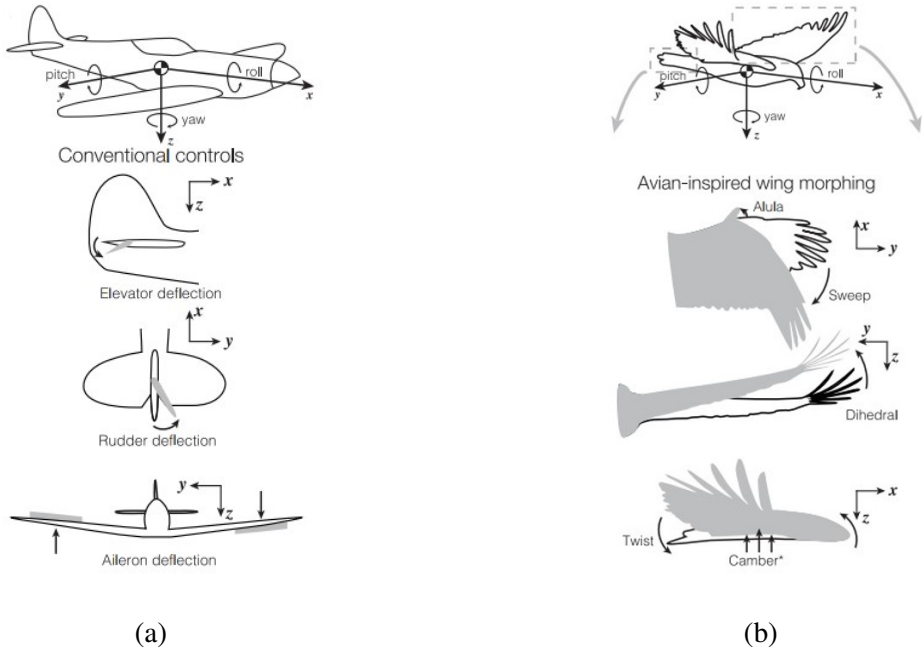


Figure 2.1: Illustration of Conventional and Avian Flight Controls (Harvey et al, 2022) [1]

drag and improve handling characteristics in manoeuvring flight[1][4]. Its effects have been studied in gust alleviation, perching manoeuvres, longitudinal and lateral control as well as stability[1], [2], [8], [22], [24] with most researches pointing to its effect in facilitating UAV recovery from obstacle impact[16]. Ajanic et al [7] observed that by extending one wing while retracting the other, wrist inspired sweep design proved effective in roll moment control even past stall. Other studies on the effect of wrist inspired wing sweep compare the effects against conventional ailerons. Chang et al [25] suggests that wrist and finger inspired wing sweep specifies the roll angle unlike traditional ailerons which tend to specify the roll rate. However a contradicting proposition exists from Di Luca et al [4] which suggests that wrist-inspired wing sweep acts similar to traditional UAV ailerons. Research predicts that backward wing sweep should increase the roll and yaw static stability [26]. The wing sweep design being considered in this research(wrist-inspired) is illustrated in Figure 2.3a showing the range of motion of the wing. The results of research in wrist-inspired wing sweep have proposed that wing sweep when actuated symmetrically can be used to achieve longitudinal control[27][8] and lateral control with asymmetric actuation as in Figure 2.3a. It has also been identified to improve stability at low speeds with effects maximised at high angles of attack[4][2][8].It has been proposed that the problem of control reversal in ailerons could be solved

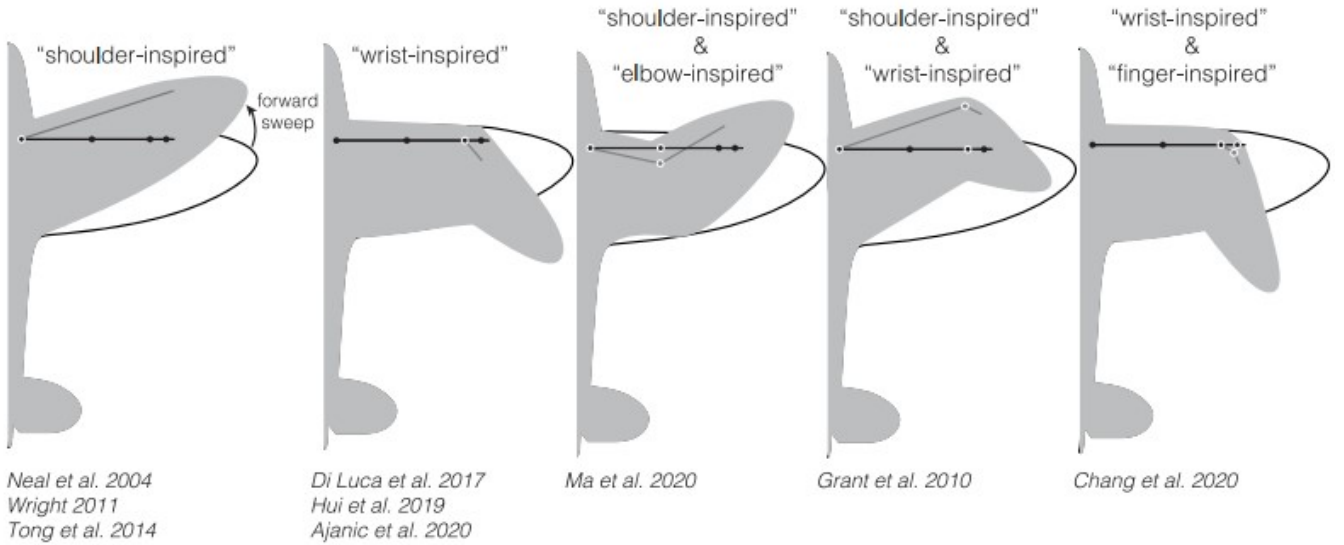


Figure 2.2: Simplified Illustrations of the Different UAV Implementations of Bio-Inspired Wing Sweep (Harvey et al, 2022) [1]

with avian inspired wing sweep[1].

Wing twist as a wing morphing mechanism is possibly one of the oldest forms of avian inspired wing morphing dating as far back as the Wright flyer[28]. Wing twist as illustrated in Figure 2.3b has been identified to function as a variable length aileron[1]. Research shows that wing root or tip twist affects the lift and drag production of a wing by shifting the zero lift angle of attack. An asymmetric, geometric or aerodynamic wing twist, can generate lift distribution on a wing resulting in a rolling moment[29][30]. Asymmetric wing twisting has been found to provide twice the roll rate than conventional ailerons with no control reversal while approaching stall conditions and reduced roll yaw coupling during roll manoeuvres[1]. When applied on a segment of the wing, research shows that wing twist has the ability to improve the aerodynamic properties of the wing at low angles of attack[3]. The effects of wing twist in drag reduction have also been highlighted [29][3] with Hunsaker proposing that the induced drag is proportional to the square of the rolling rate.

A combination of both wing sweep and and wing twist for flight control has been explored with the aim of improving the turning performance and agility of fixed-wing UAVs. Results

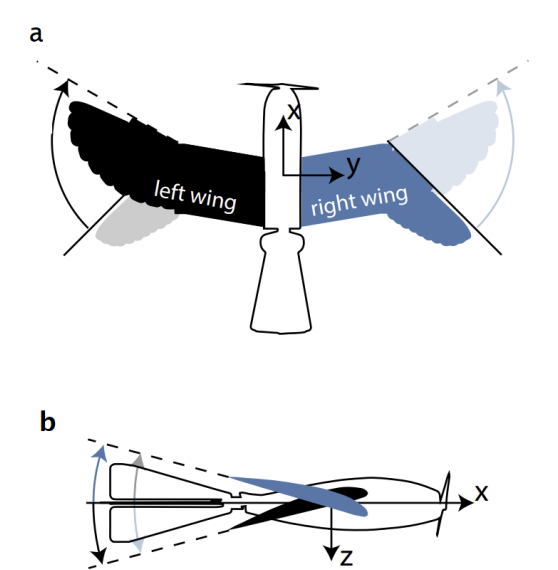


Figure 2.3: **a.** Drone illustrating asymmetric wrist-inspired wing sweep **b.** Drone illustrating asymmetric wing twist. (Ajanic et al, 2022)[6]

achieved show an increased roll rate and decreased turn radius with asymmetric wing pitching out performing asymmetric folding when rolling during cruise flight[31]. This agrees with previous research that hypothesised substantial control authority over roll and pitching moments as a product of the combination of both mechanisms[1]. Preceding research relates this mechanism combination to aggressive flight capability of the Goshawk [4][6] . Inspired by this research, this project proposes to identify the optimal degrees of actuation of the combination of both mechanisms to achieve stability in roll control while investigating the stall characteristics and control authority provided by the actuation of the wing. Although, the objectives of this report focus on analysing the benefits of implementing this mechanisms in roll control, it has been identified by previous reviews that these benefits could be extended to cruise flight stability and flapping wing drone agility[5].

It has been observed that although all avian wing joints can be implemented with variable sweep, dihedral and twist, most UAV designs tend to select one degree of freedom per joint[1], [27]. This could be due to the challenges in implementing multi degree of freedom joints. These challenges include the need to reinforce joints to account for the aerodynamic loads without significantly increasing the weight. In a study investigating the mechanism for wing sweep it was

discovered that passive redistribution of feather-like structures through an elastic connective tissue and hook shaped micro-structures on adjacent feathers aid in maintaining the aerodynamic surface during flexion and extension of the wing[32]. Application of this study can be seen in numerous researches such as Groves-Raines et al, Hui et al and Ajanic et al and Chang et al[2], [4], [6], [8], [25], [33]

3 Research Methodology

3.1 Tapered Wing Tip

The wing model dimensions used in this research as illustrated in Figure 3.1 takes inspiration from Ajanic's LisHawk [7] which had it's wingspan set within acceptable limits of the Northern Goshawk. The alterations made to the dimensions of this wing were done to suite the design objectives of this research which was to morph 40 percent of the wingspan. The decision to reduce the wing chord was made to maintain the condition that the span of the wing tip is greater than the base chord of the morphing section. A single tapered wing was used for the first iteration of the model as compared to the elliptical feather-like arrangement used in the LisHawk in order to reduce the complexity of the model. However the morphing wing tip chord(k) was chosen to provide the same plan-form area as a quad-ellipse with the same wing span and base-chord. This was done in an attempt to maintain comparability between results. Efforts were made to recreate the mod-eagle foil used in the LisHawk but it proved difficult to manufacture for the wind tunnel experiments. Therefore the JWL-065 was used throughout the wing and all models were modified appropriately to reflect this. To model realistic dimensions, the chord of the constant wing section was made slightly longer than the base-chord of the morphing section to allow movement during the sweep motion. The summary of these dimensions are shown in Table 3.1.

Dimension	Value(m)
Wing Span(b)	1.050
Root Chord	0.220
Morphing Section Base Chord(g)	0.200
Morphing section Tip chord(k)	0.114
Morphing Section Span(r)	0.210

Table 3.1: Summary of Wing Dimensions.

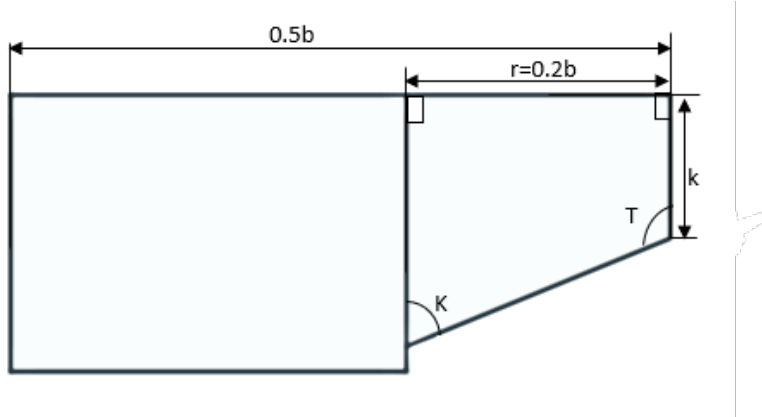


Figure 3.1: Wing Model Design Dimensions

3.1.1 Strip Theory Model

The initial modelling of the wing's aerodynamics was done using Strip Theory. This provided an approximation of the forces and moments acting on the wing. Strip Theory performs a 2D analysis of the wing by dividing it into independent strips along the span of the wing. The point of this method is that it describes the differential element of lift that is generated on a single differential strip of the wing. This modelling tool is limited as it relies on a series of assumptions which are unrealistic to simplify the model. Some of these assumptions being: the wing is operating in steady-state flight conditions, the wing's cross-section remains constant along its span including during wing sweep, there is no cross-flow across the wing.

The analysis conducted using this method focused on the rolling moment generated by differential lift caused by the sweep and twist motions of the wing tip. However, to model more realistic results, the moment generated due to the mass movement was included in the analysis. Therefore the rolling moment can be mathematically expressed as:

$$L = dL_{\Delta Lift} - dL_{\Delta cog} \quad (3.1)$$

given that $Lift = q \cdot C_l \cdot A$ where, q is the dynamic pressure , C_l is the lift coefficient, and A is the reference area.

The analysis was done for sweep angles ranging from 0 to 40 degrees for forward sweep and backward sweep and -10 to 15 degrees twist angles over a -10 to 20 range of angles of attack.

The following equations (equations 3.2 to 3.29) were used in mapping the change in sweep angle to a change in the plan-form area and the change in twist to a change in angle of attack of the twisted section.

$$A = \int_a^b f(x) dx \quad (3.2)$$

where, a and b are the span-wise limits of the section defined relative to the sweep angle and $f(x)$ if the function relating the chord variation to the points along the wing span.

C_l was represented as a function of angle of attack as shown in [34] such that:

$$C_l = a_1 \alpha + a_0 \quad (3.3)$$

where, a_1 and a_0 are constants. Therefore:

$$L = \Delta(q(a_1 \alpha + a_0)(\int_a^b x \cdot f(x) dx)) - \Delta(mg * x_{cog}) \quad (3.4)$$

where, x_{cog} is the distance of the center of gravity of the morphing section from it's root.

Note that, the rolling moment generated by the constant sections are assumed to cancel themselves out and therefore are not included in the analysis.

Backward Sweep

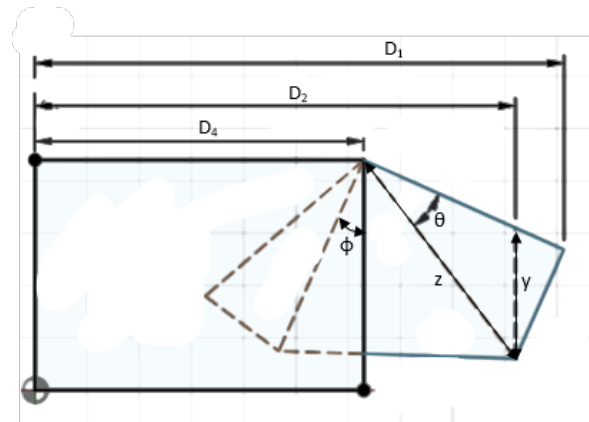


Figure 3.2: Wing Tip Backward Sweep Dimensions

Figure 3.2 illustrates the additional dimensions required for the backward wing tip sweep strip model. In this wing tip configuration, the wing tip is considered in two strips bound by the limits D_1

to D_2 and D_2 to D_4 . The dimensions were defined relative to the sweep angle using the equations below:

$$D_1 = D_4 + r \cos(\phi) \quad (3.5)$$

$$D_2 = D_4 + z \cos(\phi + \theta) \quad (3.6)$$

$$y = z \sin(\theta + \phi) - D_2 \tan(\phi) \quad (3.7)$$

$$\text{basechord} = \frac{g}{\sin(180 - \phi - K)} * \sin(K) \quad (3.8)$$

The dimensions calculated above were further used to calculate the rolling moment contributions of each strip using the equations below:

$$L_{D_2 \text{to} D_4} = q \cdot C_l \cdot \int_{D_4}^{D_2} x \cdot (mx + c) dx \quad (3.9)$$

where,

$$m = \frac{y - \text{basechord}}{D_2 - D_4}, c = y - m \cdot D_2 \quad (3.10)$$

and

$$L_{D_1 \text{to} D_2} = q \cdot C_l \cdot \int_{D_2}^{D_1} x \cdot (mx + c) dx \quad (3.11)$$

where,

$$m = \frac{-y}{D_1 - D_2}, c = -m \cdot D_1 \quad (3.12)$$

Throughout this report it was maintained that the left wing tip was varied while the right wing tip remained constant therefore;

$$L = L_{D_1 \text{to} D_2} + L_{D_2 \text{to} D_4} - L_0 + mgx_{cog}(1 - \cos \phi) \quad (3.13)$$

where, L_0 is the aerodynamic rolling moment generated by the constant wing tip.

Forward Sweep

The forward sweep was modeled using design dimensions that assume the extension emerging from beneath the wing features an isosceles plan-form with an angle equal to the maximum sweep angle being modeled (40 degrees).

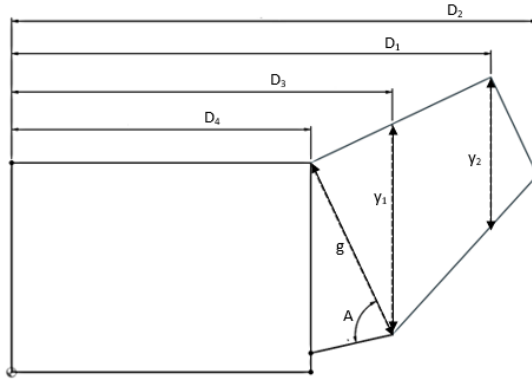


Figure 3.3: Wing Tip Forward Sweep Dimensions

Figure 3.3 illustrates the additional dimensions required for the forward sweep strip model. In this wing tip configuration, the wing tip is considered in three strips bound by the limits D_2 to D_1 , D_2 to D_3 and D_3 to D_4 . The dimensions were defined relative to the sweep angle using the equations below:

$$D_2 = D_4 + z \cos(\theta - \phi) \quad (3.14)$$

$$D_3 = D_4 + g \sin(\phi) \quad (3.15)$$

$$y_1 = g(\sin(\phi) \tan(\phi) + \cos(\phi)) \quad (3.16)$$

$$y_2 = \frac{k \sin(T)}{\sin(180 - (T + \phi))} \quad (3.17)$$

$$\text{basechord} = \frac{g}{\sin(180 - \phi - A)} * \sin(A) \quad (3.18)$$

Similarly to as presented in backward sweep, the rolling moment contributions of each strip was calculated using the equations below:

$$L_{D_3 \text{to} D_4} = q \cdot C_l \cdot \int_{D_4}^{D_3} x \cdot (mx + c) dx \quad (3.19)$$

where,

$$m = \frac{y_1 - \text{basechord}}{D_3 - D_4}, c = h - m \cdot D_3 \quad (3.20)$$

,

$$L_{D_1 \text{to} D_3} = q \cdot C_l \cdot \int_{D_3}^{D_1} x \cdot (mx + c) dx \quad (3.21)$$

where,

$$m = \frac{y_2 - y_1}{D_1 - D_3}, c = x - m \cdot D_1 \quad (3.22)$$

and

$$L_{D_2 \text{to} D_1} = q \cdot C_l \cdot \int_{D_1}^{D_2} x \cdot (mx + c) dx \quad (3.23)$$

where,

$$m = \frac{-y_2}{D_2 - D_1}, c = -m \cdot D_2 \quad (3.24)$$

therefore;

$$L = L_{D_3 \text{to} D_4} + L_{D_1 \text{to} D_3} + L_{D_2 \text{to} D_1} - L_0 + mgx_{cog}(1 - \cos \phi) \quad (3.25)$$

Twist

The model for the twist section was structured in such a way that the twist initiated from a defined point located 0.307 meters away from the wing root along the span. This arrangement is visually represented by the dimension D_5 in Figure 3.4.

From equation 3.26

$$C_l = a_1(\alpha + t) + a_0 \quad (3.26)$$

For the twisted section where, t is the twist angle.

Therefore from equation 3.4:

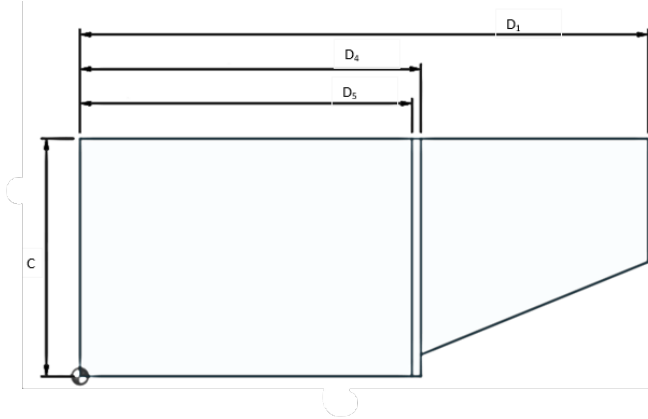


Figure 3.4: Wing Tip Twist Dimensions

$$L = q \cdot a_1(t) \left(\int_{D_5}^{D_4} x \cdot C dx + \int_{D_4}^{D_1} x \cdot (mx + c) dx \right) \quad (3.27)$$

After the individual analysis of sweep and twist were concluded, a model for the combination of sweep and twist derived from equations 3.13, 3.25 and 3.27. These can be depicted as:

For backward sweep:

$$L = q \left((a_1(t) \int_{D_5}^{D_4} x \cdot C dx) + x(a_1(\alpha + t) + a_0)(A_{D_1 to D_2} + A_{D_2 to D_4} - A_0) \right) - mgx_{cog}(1 - \cos \phi) \quad (3.28)$$

For forward sweep:

$$L = q \left((a_1(t) \int_{D_5}^{D_4} x \cdot C dx) + x(a_1(\alpha + t) + a_0)(A_{D_3 to D_4} + A_{D_1 to D_3} + A_{D_2 to D_1} - A_0) \right) - mgx_{cog}(1 - \cos \phi) \quad (3.29)$$

3.1.2 Aerodynamic Analysis Using Flow 5

Further analysis was done using Ring Vortex VLM (Vortex Lattice Method) in the Flow5 analysis. VLM's principle is to model the perturbation generated by the wing by a sum of vortexes distributed over the wing's plan-form as detailed in [35]. This method was chosen because its suitability for the scope of the research which involved sweep and twist and it's inclusion of vortex interactions as compared to Lifting Line Theory(LLT).

Ring Vortex VLM(VLM2) in Flow5 works by dividing the wing surface into panels. It places ring vortexes at the centre of each panel and horseshoe vortexes on the trailing edge of each

strip[35].These vortexes are assumed to have an effect on neighbouring panels and the interactions between the panels and the vortexes are used to calculate the aerodynamic forces on each panel. These aerodynamic Forces are summed up to obtain total lift, drag and other forces on the entire wing. Assumptions made by this method include non-viscous and non-rotational flow over the wing.

Limitations of this method include it's difficulty in accounting for wing thickness. The intersection of wing panels also create a risk of numeric instability and incorrect results.

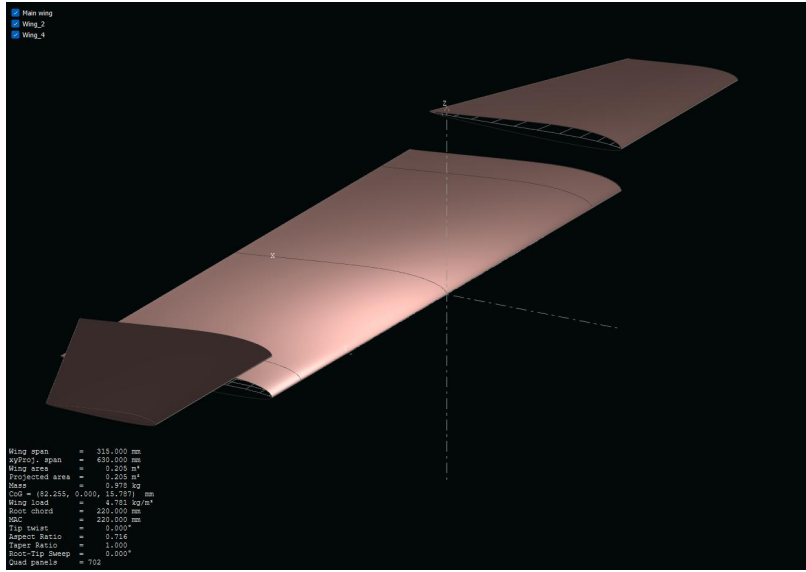


Figure 3.5: Flow 5 Wing Model for Feather-like Structured Wing Tip

The wing was modelled as shown in Figure 3.5 as a plane with three wings. The first wing represented the wing's constant section and was divided into four sections defined by the span dimensions in mm: -315,-262.5,0,262.5,315. The second and third wings represented the left and right wing tips represented as single sections with dimensions detailed in 3.1. To account for the asymmetric nature of the wings, the port side wing was initially defined as a one-sided wing, originating at the root of the 3D plane. It was then re-positioned by adjusting its span-wise axis distance. In parallel, the starboard wing was similarly configured, using an inverted JWL-065 profile about the x-axis, and then re-positioned by adjusting its span-wise axis distance and rotating it by 180 degrees about the x-axis. 13 x-panels and 9 y-panels were maintained across all sections of the 3 wings along with a cosine x-distribution and inverse sine y-distribution. A mass of 0.646kg was allocated to the constant sections while the wing tips were allocated 0.166kg each.These masses

were derived from the wind tunnel model and used to retain uniformity.

Each sweep twist combination was represented as a different plane. The sweep rotation was actuated by editing the port side wing tip's rotation about the y-axis. Twist was done by including two sections in the constant section at span-wise dimension D_5 3.4. The twist variable for the section D_5 to D_4 and the port side wing was then edited to reflect the movement. This was done to maintain consistency with the wind tunnel model.

Analysis was conducted for 0 to 40 backward sweep in 10 degree increments, -10 to 10 degrees twist in 5 degree increments and over a range of angle of attacks from -10 to 20 degrees in 0.5 degree increments for three fixed velocities: 10m/s, 12m/s and 14m/s.

In an effort to limit the effects of panel intersection during sweep the wing tips were displaced by 0.04m along the z axis. It is important to acknowledge that although this minimized the effects the accuracy of the results could still be affected.

3.1.3 Experimental Validation of Aerodynamic Results in the Wind Tunnel

In order to validate the results obtained from earlier analysis, a wind tunnel experiment was undertaken. It was important to undertake the wind tunnel modeling experiment because unlike the other two modelling techniques, wind tunnel modelling includes the effects of flow separation over the wing.

The wing model was built to utilise mounting structure already available and used in [36]. The model designed with the dimensions mentioned earlier in this report comprised of 6 sections as shown in Figure 3.6. These sections were manufactured with 3D printed PLA plastic and fit onto a 0.690m rectangular aluminium spar. This spar was assumed to provide sufficient stiffness to consider the model rigid.

The 7 by 5 feet low speed wind tunnel available within the university was used to conduct this experiment. The model was mounted to the overhead balance as shown in Figure 3.7 using two struts 0.405m apart in which the rear strut was used together with a bearing in the connecting aluminum mounting bar in varying the angle of incidence of the model from -10 to 20 degrees in 2 degree increments.

The wing tip sweep and twist angle combinations were individually 3D printed. The model was designed to facilitate the wing tips interchangeability and the right wing tip was kept constant

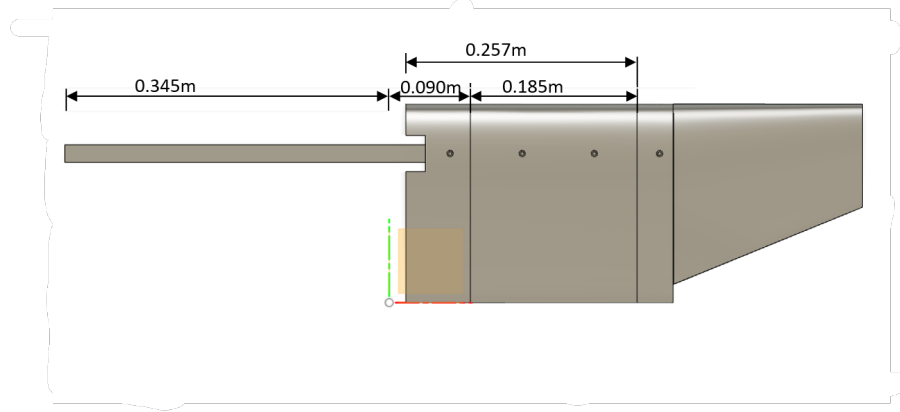


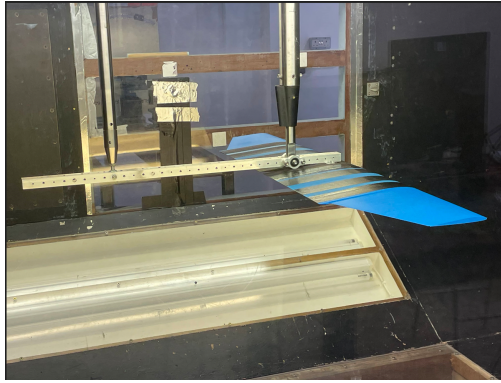
Figure 3.6: Wing Tip Twist Dimensions

throughout the experiment. Prior to the experiments the mass values of the wing components were recorded as summarised in Table 3.2. Although the masses of the normal wing tips and the constant wing section were included in the previous analysis to ensure consistency across all analyses, it is important to note that the mass distributions represented by the models were inconsistent with practical actuation of the sweep mechanism. Therefore the balance was zeroed before every iteration of the experiment in an attempt to negate the effects.

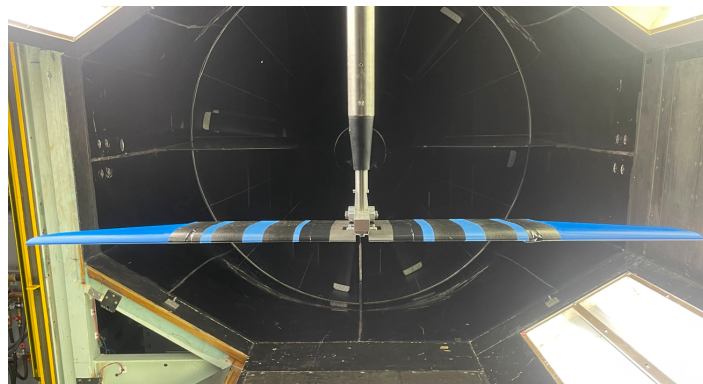
Twist	Backward Sweep		0	10	30
	Left	Right			
0	0.164kg	0.166kg	0.182kg	0.158kg	
10		N/A	0.194kg	0.196kg	
-10		N/A	0.161kg	N/A	
Constant section + Aluminium spar			0.646kg		

Table 3.2: Summary of Wing Masses.

In designing the swept wing tips, the volumetric movement was accounted for by rotating the wing tip through the desired angle and combining it with a 0.040m strip of the constant wing section. Similar methods were used to represent twist, however the twisted section was combined with a 0.032m strip of the constant section. This was done in an effort to maintain uniformity in the twisted sections. In the design of the prints for the twisted wing tip, a 5mm rolling ball fillet was



(a) Side Profile of Mounted Wing Model



(b) Frontal View of Mounted Wing Model

Figure 3.7: Wind Tunnel Setup with the Wing in Symmetrical Configuration

utilised on all edges connecting the twisted section to the constant wing section. This was done to reinforce those points and prevent them from becoming potential weak points in the wind tunnel. Duct tape was used over all gaps and holes in the model to ensure a continuous lifting surface.

Each wing tip was tested at 10, 12 and 14 m/s velocities and ten second measurements were taken at each angle of attack. Attempts were made to validate the aerodynamic models for forward sweep but the large print volume coupled with the complex geometry of the model hindered the printing process.

To further ensure accuracy in the results, the wind tunnel readings for the setup was taken without the wing model and subtracted from the other results obtained to negate its effect on the data. Finally the aerodynamic forces were normalised as follows:

$$C_D = \frac{Drag}{qA}, C_l = \frac{Lift}{qA} \quad (3.30)$$

where A was the effective area for each wing sweep angle

3.2 Feather-like Structured Wing Tip

After the analysis of the tapered wing tip, a second iteration of the model was conducted. This model focused on modeling the wing tip with realistic actuation of the wing tip sweep and twist. In this iteration, the focus was solely on backward sweep as it allowed for the precise definition of discrete plate movement. The morphing wing tip used in this model was inspired by the model analysed in [8] and was made up of three thin plates assumed to be 1.5mm thick overlapped over each other such that they formed an quad-elliptical shape when fully extended as shown in Figure 3.8. The wing tip root chord and span were maintained as 0.20 and 0.21 respectively. The plates (feather-like elements) were labeled 1 to 3 from trailing edge to leading edge. The sweep motion of the plates were defined as individual rotations about a joining pivot point set at the top inboard corner of the wing tip.

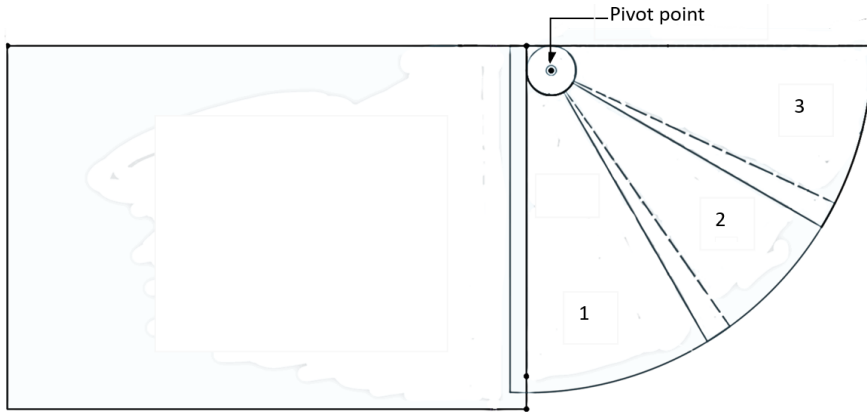


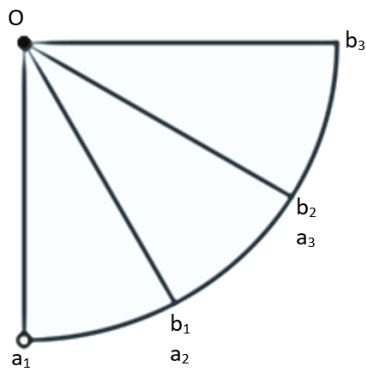
Figure 3.8: Wing Model Design for Feather-like Structured Wing Tip

The motion of the plates relative to each other was defined by the following rules:

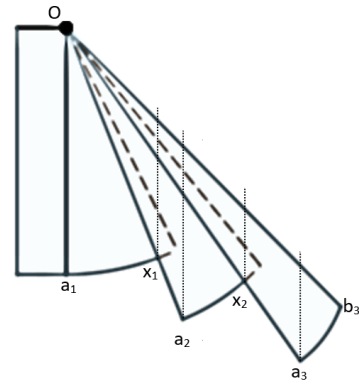
1. if $sweep \leq limitvalue$, plate 3 slides over plate 2 to actuate the sweep
2. if $sweep > limitvalue$, movement of plate 3 relative to plate 2 is equal to the limit value and plate 2 slides over plate 1 through the angle $sweep - limitvalue$

3.2.1 Strip Theory Model

In modeling the aerodynamics of this wing tip using strip theory, similar assumptions as highlighted in the sub section 3.1.1 were used. The wing and wing dimensions were represented as illustrated in Figure 3.9. The C_l used in this model were the same as those used in 3.1.1 represented as shown in equation 3.26. A uniform mass of 0.005kg was allocated to the individual plates that compose the elliptical wing tip for these calculations.



(a) Fully extended wing tip



(b) Swept wing

Figure 3.9: Strip Theory Wing Representation

The strip divisions considered in this wing tip configuration are represented by the dotted lines in Figure 3.9b. The dimensions used in this analysis are summarised in Table 3.3 For this analysis it is important to note that given a random point x : D_x is the span-wise distance of x from the wing root, y_x is the wing's chord at point x , l_x is the displacement of x from point O, $taper_x$ is the angular displacement of x from the horizontal at point O in the fully extended configuration and $x_1\hat{x}_2x_3$ is the angle between x_1 and x_3 formed at x_2 .

The rolling moment generated by the mass movement $dL_{\Delta cog}$ with respect to each plate was calculated using the equation 3.31:

$$dL_{\Delta cog} = mg(x_{cog} - \cos(taper_{cog} + \phi)) \quad (3.31)$$

Where, $\phi \leq limitvalue$ the movement was defined relative to ϕ using the following equations:

Point(x)	l_x (m)	$taper_x$ (°)
a_1	0.200	90
$b_1 = a_2$	0.200	72
$b_2 = a_3$	0.206	36
b_3	0.210	0
Angle	$Value$ (°)	
$o\hat{a}_1b_1$	81	
$o\hat{a}_2b_2$	71	
$o\hat{a}_3b_3$	71	
$a_1\hat{o}b_1$	18	
$a_2\hat{o}b_2$	36	
$a_3\hat{o}b_3$	36	

Table 3.3: Summary of Wing Dimensions for Feather-like Structures.

$$D_{b_3} = l_{b_3} \cos(\phi) + D_{a1} \quad (3.32)$$

$$y_{b_3} = 0.002m \approx 1.5mm \quad (3.33)$$

$$D_{a_3} = D_{a1} + l_{a_3} \cos(taper_{a3} + \phi) \quad (3.34)$$

$$y_{a_3} = l_{a_3} \sin(taper_{a3} + \phi) - (D_{a3} - D_{a1}) \tan(\phi) \quad (3.35)$$

$$a_2\hat{o}a_3 = a_2\hat{o}b_2 - \phi \quad (3.36)$$

$$l_{x_2} = \frac{l_{a_2} \sin(o\hat{a}_2b_2)}{\sin(180 - o\hat{a}_2b_2 - a_2\hat{o}a_3)} \quad (3.37)$$

$$D_{x_2} = D_{a1} + l_{x_2} \cos(taper_{a3} + \phi) \quad (3.38)$$

$$y_{x_2} = l_{x_2} \sin(taper_{a_3} + \phi) - (D_{x_2} - D_{a_1}) \tan(\phi) \quad (3.39)$$

As in previous sub-sections of this report the rolling moment contributions were calculated using:

$$L_{a_2toa_1} = q \cdot C_l \cdot \int_{D_{a_1}}^{D_{a_2}} x \cdot (mx + c) dx \quad (3.40)$$

where,

$$m = \frac{y_{a_2} - y_{a_1}}{D_{a_2} - D_{a_1}}, c = y_{a_2} - m \cdot D_{a_2} \quad (3.41)$$

$$L_{x_2toa_2} = q \cdot C_l \cdot \int_{D_{a_2}}^{D_{x_2}} x \cdot (mx + c) dx \quad (3.42)$$

where,

$$m = \frac{y_{x_2} - y_{a_2}}{D_{x_2} - D_{a_2}}, c = y_{x_2} - m \cdot D_{x_2} \quad (3.43)$$

$$L_{a_3tox_2} = q \cdot C_l \cdot \int_{D_{x_2}}^{D_{a_3}} x \cdot (mx + c) dx \quad (3.44)$$

where,

$$m = \frac{y_{a_3} - y_{x_2}}{D_{a_3} - D_{x_2}}, c = y_{a_3} - m \cdot D_{a_3} \quad (3.45)$$

and

$$L_{b_3toa_3} = q \cdot C_l \cdot \int_{D_{a_3}}^{D_{b_3}} x \cdot (mx + c) dx \quad (3.46)$$

where,

$$m = \frac{y_{b_3} - y_{a_3}}{D_{b_3} - D_{a_3}}, c = y_{a_3} - m \cdot D_{a_3} \quad (3.47)$$

therefore:

$$dL_{\Delta Lift} = L_{a_2toa_1} + L_{x_2toa_2} + L_{a_3tox_2} + L_{b_3toa_3} - L_0 \quad (3.48)$$

Furthermore , where, $\phi > limitvalue$ the movement was defined relative to ϕ using the following additional equations:

$$a_2 \hat{a}_3 = a_2 \hat{b}_2 - limitvalue \quad (3.49)$$

$$a_1 \hat{o} a_2 = a_1 \hat{o} b_1 - \phi + limitvalue \quad (3.50)$$

$$D_{a_2} = D_{a_1} + l_{a_2} \cos(taper_{a_2} + \phi - limitvalue) \quad (3.51)$$

$$y_{a_2} = l_{a_2} \sin(taper_{a_2} + \phi - limitvalue) - (D_{a_2} - D_{a_1}) \tan(\phi) \quad (3.52)$$

$$l_{x_1} = \frac{l_{a_1} \sin(o\hat{a}_1 b_1)}{\sin(180 - o\hat{a}_1 b_1 - a_1 \hat{o} a_2)} \quad (3.53)$$

$$D_{x_1} = D_{a_1} + l_{x_1} \cos(taper_{a_2} + \phi - limitvalue) \quad (3.54)$$

$$y_{x_1} = l_{x_1} \sin(taper_{a_2} + \phi - limitvalue) - (D_{x_1} - D_{a_1}) \tan(\phi) \quad (3.55)$$

and the additional rolling moment contributions were:

$$L_{x_1 to a_1} = q \cdot C_l \cdot \int_{D_{a_1}}^{D_{x_1}} x \cdot (mx + c) dx \quad (3.56)$$

where,

$$m = \frac{y_{x_1} - y_{a_1}}{D_{x_1} - D_{a_1}}, c = y_{a_1} - m \cdot D_{a_1} \quad (3.57)$$

and

$$L_{a_2 to x_1} = q \cdot C_l \cdot \int_{D_{x_1}}^{D_{a_2}} x \cdot (mx + c) dx \quad (3.58)$$

where,

$$m = \frac{y_{a_2} - y_{x_1}}{D_{a_2} - D_{x_1}}, c = y_{a_2} - m \cdot D_{a_2} \quad (3.59)$$

therefore;

$$dL_{\Delta Lift} = L_{x_1 to a_1} + L_{a_2 to x_1} + L_{x_2 to a_2} + L_{a_3 to x_2} + L_{b_3 to a_3} - L_0 \quad (3.60)$$

3.2.2 Aerodynamic Analysis Using Flow 5

In Flow5 the wing was modelled as 7 wings with the constant section represented as shown in Figure 3.10. Each feather-like structure was represented as 0.01m strips of varying chord length and offset values arranged in order. Similar movements and rotations were performed on the wing tips as detailed in the previous subsection to account for the asymmetric nature of the wings.

Key differences between both models include that: a symmetric 1.5mm flat plate profile was used across all sections of the feather-like structured wing tip, an equal mass 0.09kg were given to all feather-like structures and the mass of the constant section was 0.42kg, accross all 6 feather-like structures 13x-panels and 7 y-panels were used along with a cosine x-distribution and uniform y-distribution.

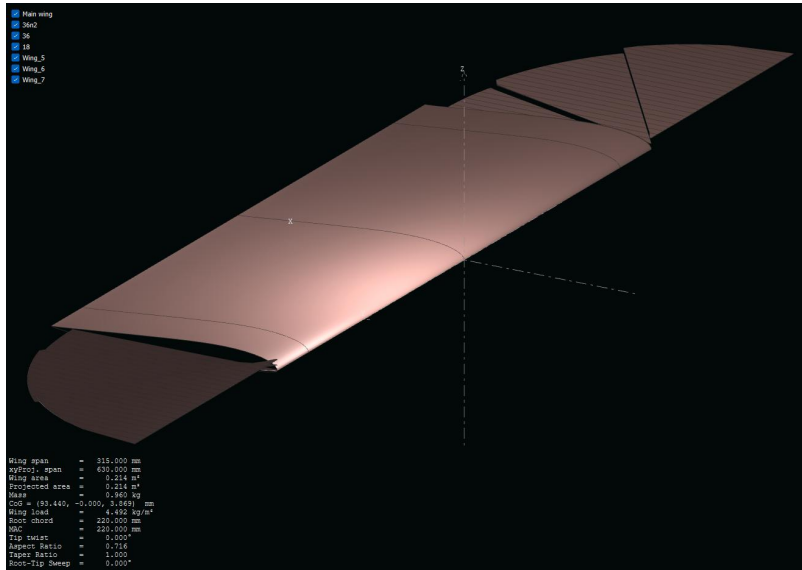


Figure 3.10: Flow 5 Wing Model for Feather-like Structured Wing Tip

As done in the first iteration of this research, Ring Vortex VLM was used in the aerodynamic analysis of the wing model. Each sweep twist combination was represented as a different plane. the sweep rotation was actuated following the rules stated earlier in this section. The data ranges used in 3.1.2 were maintained in this analysis.

In an effort to limit the effects of panel intersection during sweep the feather-like structures were ordered 5mm apart along the z axis.

4 Results

In presenting the results of this study, it is essential to establish a clear understanding of the sign conventions used in the presentation of data. In the representation of sweep angles, negative(-ve) angles represent backward sweep while (+ve) angles represent forward sweep. Similarly negative twist angles represent a nose down twist while positive twist angles represent nose up twist. As earlier stated in previous chapters, these wing morphing mechanisms were applied to the wing tip which constituted 20 percent of the wing span as shown in Figure 3.1 and Figure 3.8

4.1 Tapered Wing Tip Aerodynamic Model Data

The following results were generated using the Strip Theory model and Flow 5 aerodynamic analysis tool:

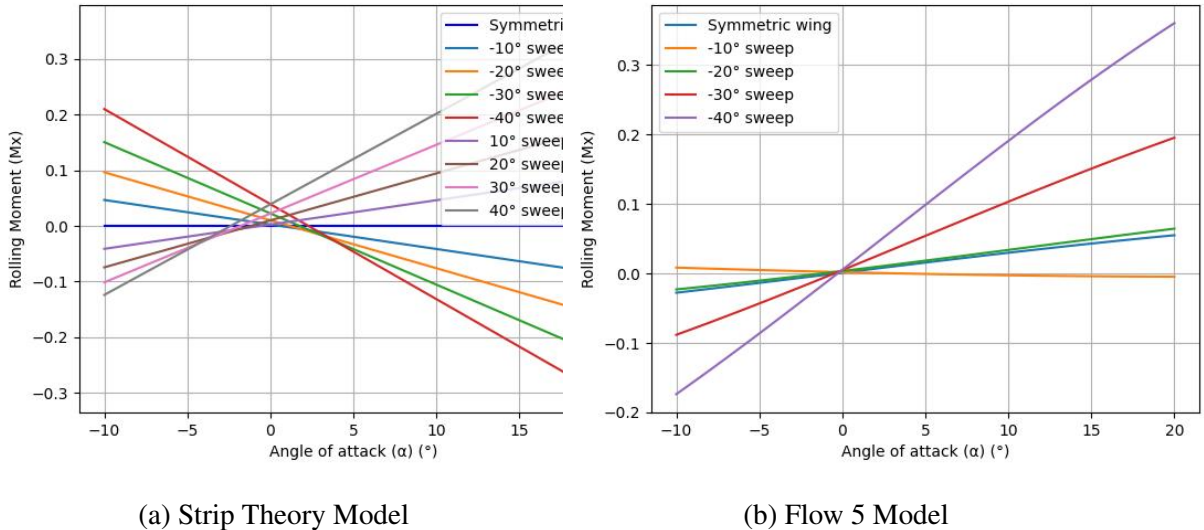


Figure 4.1: Rolling Moment (Nm) vs. Angle of Attack ($^{\circ}$) for Varying Sweep Angles at 12m/s

The strip theory model in Figure 4.1a exhibits a constant zero rolling moment for the symmetric wing configuration, which aligns with expectations. In this configuration both wingtips are identical

resulting in the equilibrium of the rolling moment due the weight and lift forces on both sides of the wing.

The Flow 5 model shown in Figure 4.1b on the other hand shows a slight unexpected positive incline in the rolling moment for the symmetric wing configuration. This observation raises the possibility of discrepancies in the aerodynamic tool's data. However, it is essential to note that each wing configuration was treated as a separate entity in the modeling process. Therefore, any discrepancies or errors should be attributed solely to the specific trend represented by that configuration, rather than generalized to all models. However, both models show a change in the lateral static stability of the model as the sweep angle is varied.

The strip theory model suggests that the wing model tends to be more laterally unstable as the wing tip extends forward as evidenced by the positive trend in the graph. Conversely, the model shows increased stability as the wingtip is retracted backward. This behaviour can be attributed to the wing tips change in area as the differential lift forces generated tends to roll the wing in the direction of the most retracted wing tip at high angles of attack. The strip theory model also depicts an increase in the value of the linear curves intercept with the rolling moment axis at 0 degrees angle of attack regardless of the sweep direction. This can be suggested to be the effect of the mass movement which acts to contradict the differential lift with increase in sweep angle. The results shown in Figure 4.1a also show that for lower angles of attack which as depicted in this figure ranges between -2 degrees to +2 degrees, wing tends to roll in the direction of the morphed wing tip regardless of the direction of sweep. this range can be increased or decreased by adjusting the weight of the wing tip.

The Flow 5 model however shows negligible variation in the rolling moment at 0 angle of attack. This seems to suggest that the effect of the mass movement is relatively insignificant compared to the differential lift generated by the sweep movement. It also suggests that for a wing swept backward further than 10 degrees the wing's reaction tends to lateral instability. This contradicts the results obtained from the strip theory model. Reasons for this contradiction could include the difference in the representation of the wing tip retraction in both models as the retracted section of the wing still visible in the flow 5 model. This could introduce errors in the results presented. The flow 5 model also depicts a slight negative difference in the magnitude of the moment from those depicted by the strip theory model . This is most likely related to error in the lift coefficient used for

the calculations of swept wing forces and moments highlighted later in this chapter and illustrated in Figure 4.3a.

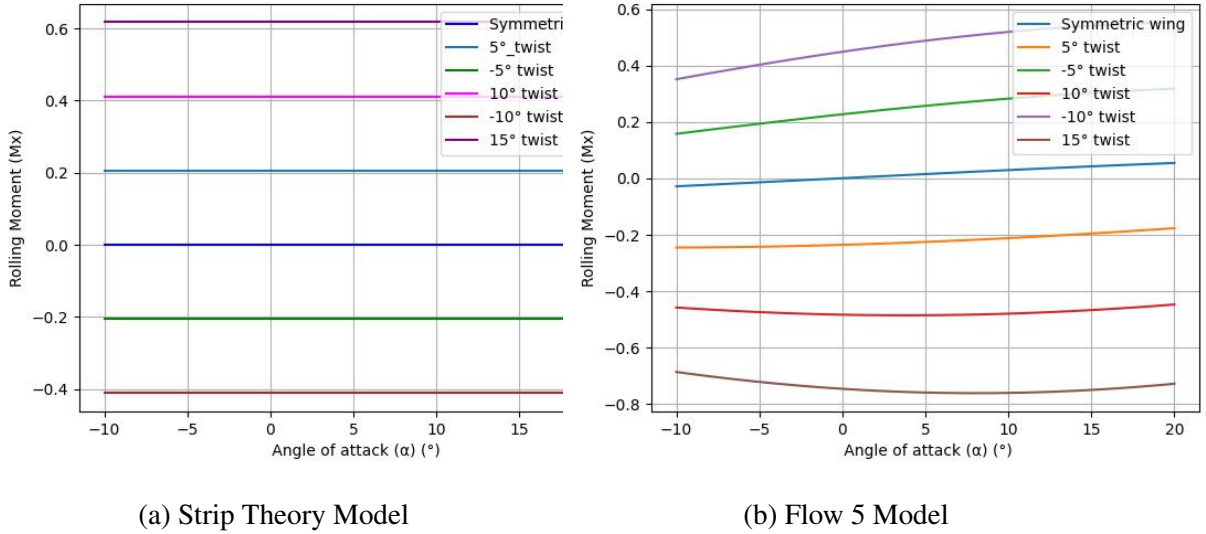


Figure 4.2: Rolling Moment (Nm) vs. Angle of Attack ($^{\circ}$) for Varying Twists Angles at 12m/s

Similarly, both models agree in the trend observed when twisting the wingtip, as shown in Figure 4.2. They both depict a constant difference in the rolling moment generated regardless of changes in angle of attack. However, it is worth noting that there exists a difference in the magnitude of the forces generated by the flow 5 model as previously mentioned. This discrepancy can be attributed to factors mentioned earlier, such as vortex reactions and Flow 5's ability to model a more precise aerofoil variation for sweep motion, which are not accounted for in the strip theory model. Moreover, it's crucial to highlight that while both models show a consistent trend in terms of the difference in rolling moment, the directions of the moments are reversed between the two models. After reviewing the sign conventions presented in the software's recommended handbook [35], it was proposed that this is most likely due to a sign error in the Flow 5 analysis tool.

4.1.1 Results of Tapered Wing Tip Model Comparison Against Wind Tunnel Data

Lift and Drag analysis

While collating data from the wind tunnel experiments, it was identified that during the measurement of the results for the -10° swept wing model, the overhead balance had not been properly zeroed before the commencement of the experiments. This introduced an element of uncertainty regarding the absolute magnitudes of the results obtained from this specific wing model. To address this issue, the data error generated associated with this wing model was assumed to be a constant non-zero error due to the nature of the results. While this assumption acknowledged the disputable magnitudes, it also recognized the significance of the observed trend within the data. This trend was deemed crucial for the comprehensiveness of the results discussed in this research. As a means of highlighting the uncertainty in magnitude, this trend has been represented in the graphs as a red dotted line.

In the results below, solid lines are used in the representation of wind tunnel data while dashed lines are used to represent the data being compared.

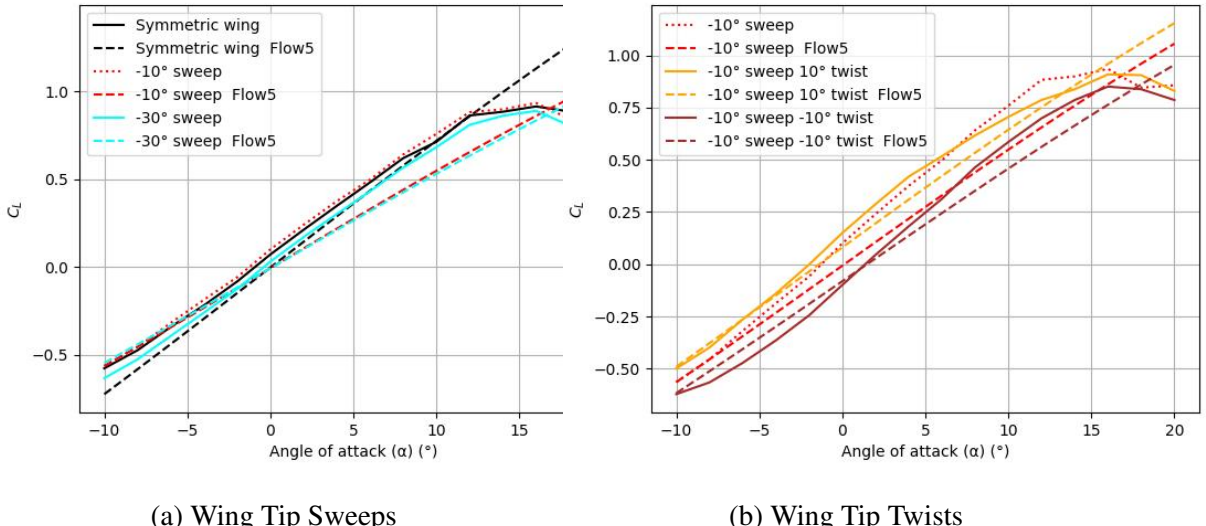


Figure 4.3: Lift Coefficient vs. Angle of Attack ($^\circ$) at 12m/s: Wind Tunnel Data vs Flow 5 Data

The results in the C_L vs α graph illustrated in Figure 4.3a show a constant difference in the

wind tunnel data magnitudes of C_L for the symmetric wing section and the wing with -30° wing tip sweep. This difference aligns with expectations which suggest that the change in the aerodynamic profile of the retracted wing tips could slightly alter the lift coefficient of the wing.

One notable distinction between the wind tunnel data and the Flow 5 data set is the wind tunnel's ability to model flow separation along the model. These regions of flow separation can be observed in the plots as the non linear regions. Flow separation can be seen to occur within the same region of ±16 degrees for all wing models. While flow separation is evidently pronounced at high angles of attack, the slight curve noticed at the base of the plots which is most evident in the -10° sweep -10° twist plot in Figure 4.3b indicates the likelihood of flow separation at extremely low angles of attack as well.

Figure 4.3 provides information that can help to shed light on the source of some of the possible differences between the models and the wind tunnel data. In the data illustrated in Figure 4.3a it can be observed that while the slope in the C_L graphs for the symmetric wing configuration seem to agree, a significant deviation can be seen in the C_L graphs for the wings with swept wing tips. These could be attributed to the analysis tool not properly representing the wing camber transformations during sweep. It is essential to note that the C_L value used for the strip theory model was derived only from the symmetric wing. Therefore, the effect of this deviation might only be seen in the Flow 5 data.

Having established that the slope estimation of the swept wing in Flow 5 is different from the wind tunnel data, It can be observed that the reaction to the change in wing tip twist is consistent with the estimates of the Flow 5 model as an increase in magnitude can be observed for the positive twist angle while a decrease can be observed from the negative twist.

The relationship between C_D and angle of attack α for both wind tunnel and Flow 5 data is illustrated in Figure 4.4. While the Flow 5 model generally underestimates the drag produced by the model, A key difference between the models can be observed in Figure 4.4a; the Flow 5 model predicts a zero minimum value for all sweep wing tip sweep angles as compared to the non-zero minimum values shown in the Wind Tunnel data.

The wind tunnel data can be considered to be the more realistic of the two drag representations, as even at zero degree angles of attack, the wing's leading edge area remains oriented facing the fluid stream, thus implying the presence of some expected drag. The difference in the minimum

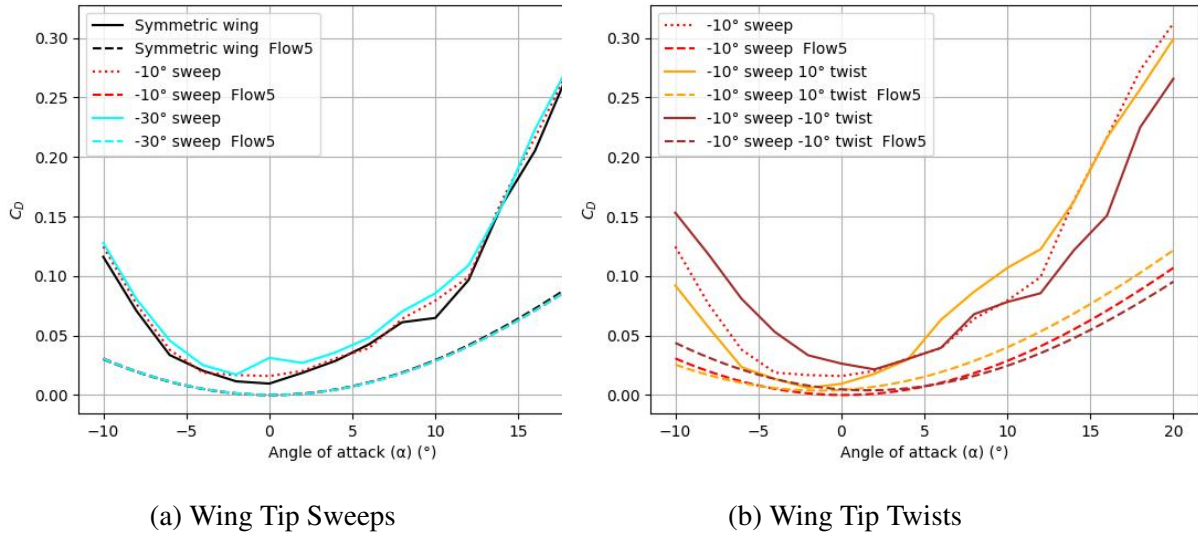


Figure 4.4: Drag Coefficient vs. Angle of Attack ($^{\circ}$): Wind Tunnel Data vs Flow 5 Model at 12m/s

values of C_D for the change in wing tip sweep suggests that the change in the wing tips aerodynamic profile generates a variation in the drag produced at low angles of attack.

Notably, a major similarity in the trends can be seen in Figure 4.4b where the line crosses can be seen to be nearly identical between the two models. These intersections can be hypothesized to stem from the difference in the angles of attack in which the wing models with twisted wing tips experience minimum drag forces. It becomes apparent that these intersections lie along the angle of attack axis, positioned in the direction opposite to the incidence of the twisted wing tip.

Moment Analysis

The wind tunnel model of the symmetric wing displayed an unexpectedly high rolling moment as shown in Figure 4.5. This deviated significantly from the predictions of all models and contradicted anticipated real-world behaviour. Possible reasons for this irregularity in the data which indicates a constant positive rolling moment at all angles of attack include that: the zeroing of the balance may have gotten rid of constant errors in the data but not the mass differences between both wing tips as earlier indicated in Table 3.2, there could be asymmetry in the aluminium spar running through the model causing a constant rolling moment to the right.

Another irregularity shown in Figure 4.5 between the wind tunnel data and both models is the

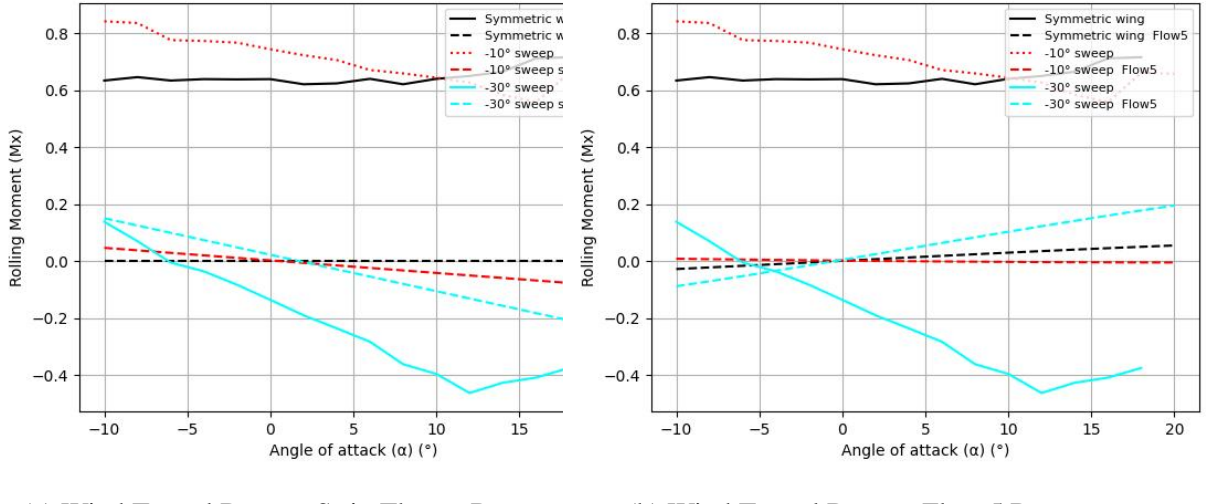


Figure 4.5: Rolling Moment (Nm) vs. Angle of Attack ($^{\circ}$) for Varying Sweep Angles at 12m/s

slope of the rolling moment generated by the wing tip sweep morphing. The most likely reason for this being that: given the more realistic depiction of the effects of the aerodynamic profile change during wing sweep by the wind tunnel data,a greater negative moment due to differential lift than predicted by both models is generated.This possibility is supported by the trend shown in Figure 4.3a. The wind tunnel data suggests that for wing tip sweep there tends to be a greater variation in the lateral stability of the model than earlier predicted by the strip theory and Flow 5. Also, given that the wind tunnel model is assumed not to take into account the mass distribution that opposes the differential lift as done by the other two models, the magnitude of the forces generated by the model with the -30° retracted wing tip is greater than those depicted by the strip theory data. Finally, the change in direction of the wind tunnel line at 12° angle of attack coincides with the onset of stall in Figure 4.3a

The overall trend observed in the strip theory and wind tunnel data however suggests that the wing model tends to be more laterally stable as the wing tip is being retracted. This agrees with results proposed by Chin 2017 [16]and Ajanic 2023[31].

Although the data obtained from the Flow 5 model illustrated in Figure 4.5b shows a variation in the lateral stability of the wing with wing tip sweep, it opposed the data generated by the other two models. Reasons for this could be a sign error in the analysis software resulting in an error

generated when calculating rolling moments. This exact error can also be seen in Figures 4.2b and 4.6b. Due to this observation, it was considered to be an unreliable tool for modelling the rolling moment generated by the wing tip sweep.

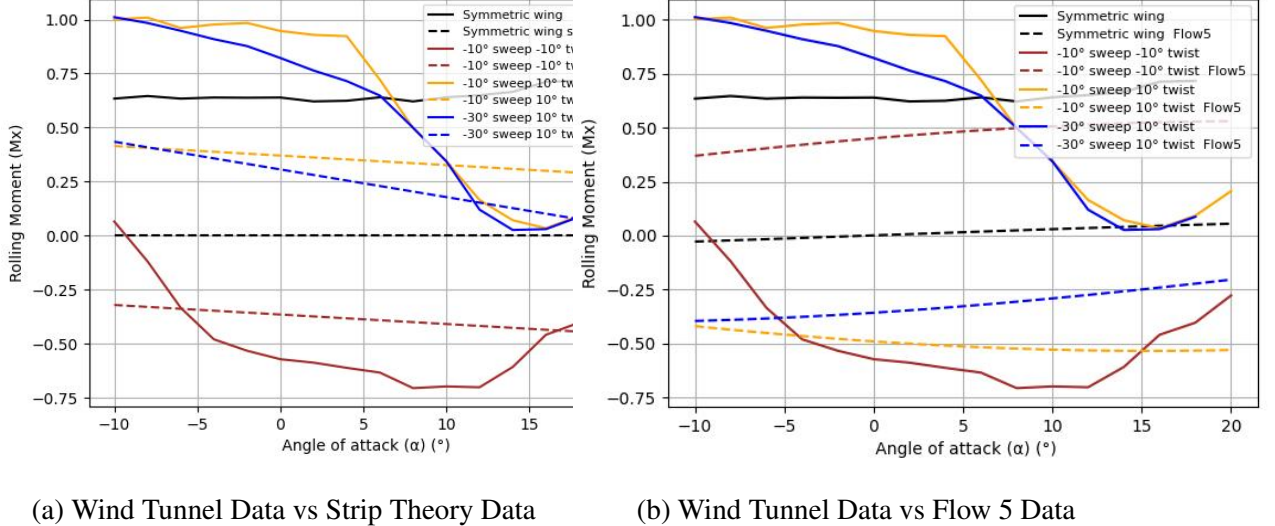


Figure 4.6: Rolling Moment (Nm) vs. Angle of Attack ($^{\circ}$) for Varying Sweep and Twist Angles at 12m/s: Wind Tunnel Data Comparisons

The wind tunnel data for wing twist on the other hand as shown in Figure 4.6a agrees with the strip theory model's depiction of wing twist morphing except at the regions where the onset of flow separation is noticed as identified previously in Figure 4.3b. Both wing models with 10° twist can be seen to have produce rolling moments with a linear relationship with angle of attack before a sudden change in slope is observed at approximately 5° angle of attack. This reaction suggests that at $5^{\circ} \alpha$ the twisted wing tip experiences flow separation. This results in a decline in the differential lift force generated as the constant wing tip continues to experience increased lift force. This can also be seen in Figure 4.3b as the slight change in slope of the C_L vs α curve. A curve is then seen at approximately 15° where the rolling moment tends to increase. This point suggests the onset of stall on the constant wing tip.

Similarly, the wing model with -10° wing tip twist experienced similar slope changes at -4° and $12^{\circ} \alpha$. The data before $-4^{\circ} \alpha$ suggests there is flow separation at the twisted wing tip while the data after $12^{\circ} \alpha$ suggests that the constant wing is experiencing flow separation. This was inferred after

identifying the incidence angles of the wing tips to the flow stream at these points. Based on this inference it can be hypothesised that the range of values for which the strip theory model defines the wind tunnel data can be modified by modifying the degree to which the wing tip is twisted.

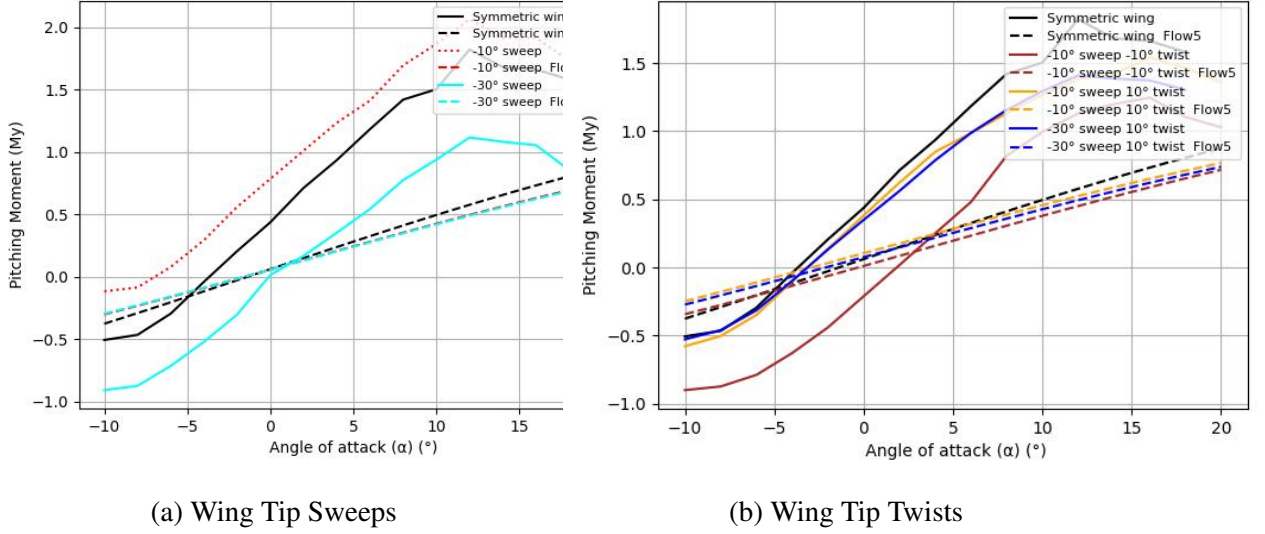


Figure 4.7: Pitching Moment (Nm) vs. Angle of Attack ($^{\circ}$): Wind Tunnel Data vs Flow 5 Data at 12m/s

The results in Figure 4.7 illustrate the relationship between pitching moment and wing tip sweep and twist for varying angles of attack. The results in Figure 4.7a show a general decrease in pitching moment generated by the wind tunnel wing models with increase in wing tip backward sweep. This can be said to be related to the reduction in the lift coefficient of the models as earlier highlighted in this chapter. These results tend to mimic those seen in Figure 4.3a. However the deviation in the data between the wind tunnel data the Flow 5 data seems to be greater in Figure 4.7. this is suspected to be due to the differences in the points about which the pitching moments were recorded for both models. The Flow 5 data generates its pitching moment values about the mass centre of the model which was displaced due to the alterations mentioned in Section 3.1.2 of this report. These alterations were made in an attempt to model realistic vortex reactions.

This reduction in the pitching moment seen to be consistent in models with retracted wing tips tends to be made up for by an increase in the twist(incidence)of the retracted wing tip at lower angles of attack as illustrated in the data represented in Figure 4.7b. It is however observed that

as the twisted wing tip approaches the stall angle as earlier highlighted, the pitching moment of the wing models with retracted wing tips deviate significantly from the values of the symmetric wing model until the constant wing section stalls at higher angles of attack. Similarly the loss of incidence on the -10° twisted wing tip results in the overall reduction of the pitching moment generated. The increase and decrease in the pitching moment due to the respective changes in the wing tip's incidence to the flow can be seen to be reflected in the Flow 5 model. These variations in the pitch moment suggest that the wing model will experience variations in its pitch trim position in flight with variation in wing tip twist and sweep. These results present trends similar to the results of the research done on asymmetric wing tip twist by Young 2023 [30]

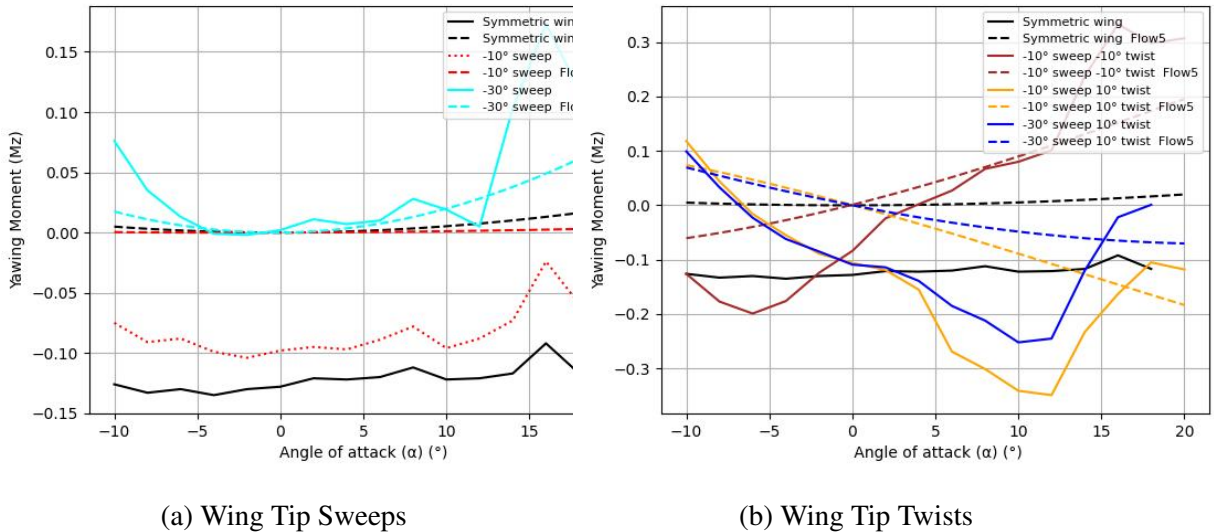


Figure 4.8: Yawing Moment (Nm) vs. Angle of Attack ($^\circ$) for Varying Twist Angles at 12m/s: Wind Tunnel Data vs Flow 5 Data

The yaw moments generated by the wind tunnel models are illustrated in Figure 4.8 alongside the Flow 5 trends predicted for the models. The constant yaw moment shown in the symmetric model suggests an asymmetry in the 3-D printed model or the wind tunnel used in this research. Given the research presented in [37] the later is more likely. However in the interpretation of these results, this line was considered to be the wing model's normal. In Figure 4.8a it can be seen that the wind tunnel data and Flow 5 data indicate an increased yawing moment as the wing approaches really high and really low angles of attack for retracted wing tip configurations. This suggests that

the difference in the areas of the wing tips incident to the air flow increases as the wing approaches extreme incidence angles. The constant difference in the yawing moment reflected in the wind tunnel data suggests that the wing model tends to yaw in the opposite direction of the morphed wing tip during wing tip retracted sweep. The earlier identified error in representing the leading edge's area incidence to the flow explains why this yawing moments are shown to be zero in the flow 5 model.

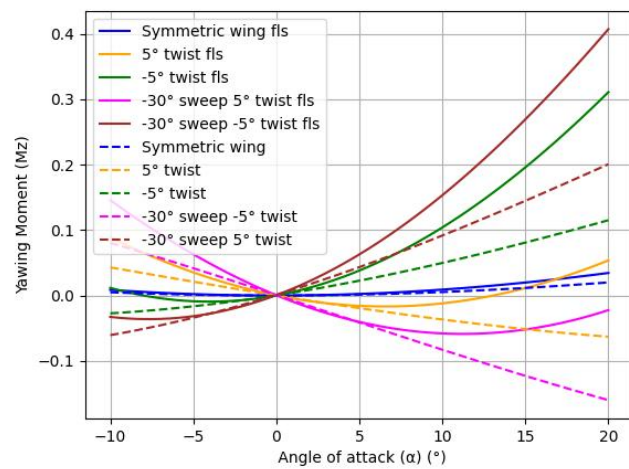
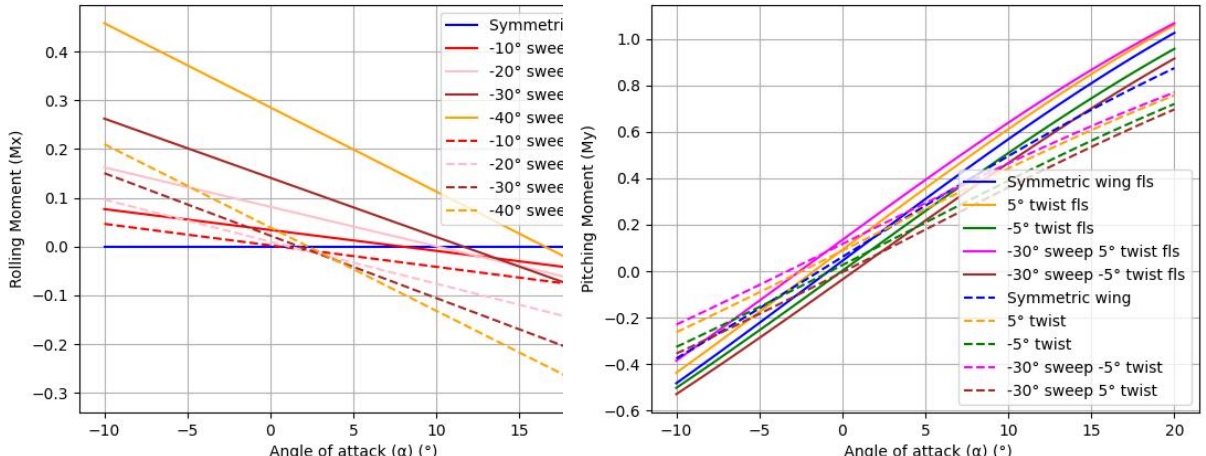
The yawing moment generated by the twisted models as presented in Figure 4.8b suggests that for the wing model with a nose down twisted wing tip, the wing model tends to yaw in the direction of the morphed wing tip at negative angles of attack. This moment tends to turn to zero as the wing model's angle of attack is varied and turns to positive as the angles of attack of the model turns positive. Similar but opposite moments can be seen on the wing models with positively twisted wing tips. This suggests that the wing model tends to yaw in the direction of the morphed wing tip with increase in incidence in the direction of the wing morphing due to a difference in the drag forces experienced on both wing tips resulting in a turning moment in the direction of the morphed wing tip. However as the angle of attack turns to zero the drag forces on wing tips tend to balance out resulting in the yawing moment returning to zero. Similarly the yawing moment turns in the direction of the constant wing as the angle of attack of the wing model opposes the twisted wings incidence. It is however important to note that the yawing moment with respect to the direction is less for the more retracted wing tip. This suggests that due to the retraction of the wing's area, more of the wing's drag forces acts to oppose thrust than yaw the wing model. This proposition is consistent with the variation in drag seen in Figure 4.4a for the same angles of attack showing obvious variation in Figure 4.8b.

4.2 Comparison of Results of Feather-like Structured Wing Tip Model Against Tapered Wing Tip Model

The results illustrated in Figure 4.9 illustrate the differences in the force and moment reactions between the feather-like structured wing tip and the tapered wing tip discussed in this report. It is however important to note that the magnitudes of the forces and moments presented in these results could be misleading as the masses allocated to the feather-like elements do not agree with

realistic expectations. However the results generated by these models act as an approximation of the reactions to be expected by using this wing tip structure.

The results represented in Figure 4.9 show that the change in wing tip sweep actuation of the wing model does not significantly affect the nature of the aerodynamic reactions gotten from the retraction of the wing tip. However the difference in the magnitude of the moments generated in the strip theory model for the feather-like structured wing tip in Figure 4.9a can be attributed to the difference in the mass movement during the wing tip sweep motion. Realistically, these effects are expected to be negligible. The data shown for the feather-like structured wing tip in Figure 4.9b and 4.9c however seem to provide comparisons that reflect the wind tunnel data better than seen in the tapered wing tip model.



(c) Flow 5 Model for Yawing Moment (Nm) vs. Angle of Attack ($^{\circ}$)

Figure 4.9: Data Comparison For Feather-Like Structured Wing Tip vs Tapered Wing Tip

5 Discussion and Conclusion

5.1 Research Summary

Bio-Inspired wing morphing could render solutions to current challenges hindering the application of fixed wing in missions that require high degrees manoeuvrability and involve urban environments. The research presented in this report modelled the aerodynamic forces and moments generated by a bio-inspired wing using wing tip sweep and twist as flight control mechanisms in fixed wing UAVs. This was achieved by designing a wing model and performing strip theory and aerodynamic analysis on the model for different degrees of wing tip sweep and twist over a range of angles of attack.

The results presented in this dissertation suggest an overall loss of lift force generated with increased retraction of the wing tip. An increase in the drag force generated due to change in the aerodynamic profile of the wing tip during retraction can also be observed. Wing tip twist however can be observed to generate constant differences in the lift forces generated with respect to the direction of the morphing motion. However a slight tilt in the direction of the lift coefficient versus α curve can be observed at angles where the twisted wing tip is expected to experience flow separation. Similar variations as seen in the lift force can be observed in the pitching moment as well. These reactions generated by the wing tip twist can be corroborated by research shown in Young 2023 [30]

The Data also suggests that asymmetric wing tip sweep generates large rolling moments at high angles of attack and varies the lateral stability of the model. Asymmetric wing tip twist on the other hand generates a constant rolling moment. A combination of both mechanisms can be predicted to allow for the generation of large correcting moments to offset the effects of gust disturbance . This suggests the possibility of changing between extremely stable and more agile wing configurations during flight. However variation in wing tip twist affects the range of linearity in model reaction to control input due to the flow separation characteristics of the wing model. These results agree with

the results presented by [16] and [6]. The results also suggest that the yawing moment generated by both mechanisms are a function of the difference in the area of both wing tips incident to the wind direction.

This research further suggests possible actuation of the wing tip morphing mechanisms considered and illustrates that for the specific feather-like structures considered there is no significant deviation in the nature of the reactions expected as indicated by the analysis methods used.

5.2 Research Limitations

The following are the critical limitations of this research selected from those observed and highlighted in earlier chapters of this report where deemed necessary:

1. A major hole in the results presented by this report is the absence of significant modelling of the reactions expected by forward wing tip sweep.
2. The wing model presented in this report was not optimised for flight.
3. Steady State flight conditions were assumed were assumed in the development of the presented models and results

5.3 Research Applications and Impact

The data presented in this research indicates that these bio-inspired mechanisms can be used for flight control. It serves to provide information regarding the variation in control authority provided by these mechanisms at low speeds for different degrees of actuation and high angles of attack. This information contributes to the research advancement directed at the application of bio-inspired wing morphing in fixed wing UAV design, especially as it pertains to wing tip twist and sweep. The impact of this contribution lies in its proposed improved agility and stability of fixed wing UAVs. These properties have been identified by research shown in [12] to be vital in manoeuvring in environments with high levels of turbulence, adverse weather conditions (gusts) and clutter.

These properties can be applied in increasing the energy and cost efficiency of performing UAV related tasks in urban environments which most commonly uses multi rotor drones due to their cur-

rently higher levels of manoeuvrability and stability. Other applications of this proposed improvements to fixed wing UAVs include an improvement in military defensive manoeuvres, combat, surveillance and search and rescue operations.

5.3.1 Further Research

Further research needs to be done before the mechanisms proposed in this research can be considered safe and reliable to be implemented in fixed wing UAVs. Possible progressions in these research involve:

- Developing more detailed aerodynamic results for the extended wing tip configuration(forward wing tip sweep),
- Redoing the wind tunnel experiment eliminating all errors highlighted in this report, especially for the wing model with -10 degrees retracted wing tip and no twist,
- Validating the aerodynamic results for the feather-like structured wing tip through wind tunnel experiments, using realistic mass distributions,
- Optimising the wing designs for flight and observing the reactions due to moment couplings generated by the bio-inspired mechanisms,
- Analysing the effect of the number of feather-like structures as well as frequency of actuation of these morphing mechanisms on the aerodynamic moments generated,
- Validating the proposed increased agility offered by this design against conventional control surfaces to confirm the necessity for the increased mass penalty and complexity in design associated with implementing both mechanisms.

References

- [1] C. Harvey, L. L. Gamble, C. R. Bolander, D. F. Hunsaker, J. J. Joo, and D. J. Inman, A review of avian-inspired morphing for uav flight control, *Progress in Aerospace Sciences* [online], vol. 132 2022, p. 100 825, 2022, ISSN: 0376-0421. DOI: <https://doi.org/10.1016/j.paerosci.2022.100825>. available from: <https://www.sciencedirect.com/science/article/pii/S0376042122000173>.
- [2] Z. Hui, Y. Zhang, and G. Chen, Aerodynamic performance investigation on a morphing unmanned aerial vehicle with bio-inspired discrete wing structures, *Aerospace Science and Technology* [online], vol. 95 2019, p. 105 419, 2019, ISSN: 1270-9638. DOI: <https://doi.org/10.1016/j.ast.2019.105419>. available from: <https://www.sciencedirect.com/science/article/pii/S1270963819315731>.
- [3] H. Rodrigue, S. Cho, M.-W. Han, B. Bhandari, J.-E. Shim, and S.-H. Ahn, Effect of twist morphing wing segment on aerodynamic performance of uav, *Journal of Mechanical Science and Technology* [online], vol. 30, no. 1 2016, pp. 229–236, 2016, ISSN: 1976-3824. DOI: [10.1007/s12206-015-1226-3](https://doi.org/10.1007/s12206-015-1226-3). available from: <https://doi.org/10.1007/s12206-015-1226-3>.
- [4] M. Di Luca, S. Mintchev, G. Heitz, F. Noca, and D. Floreano, Bioinspired morphing wings for extended flight envelope and roll control of small drones, *Interface focus*, vol. 7, no. 1 2017, p. 20 160 092, 2017.
- [5] S. Tanaka, A. Asignacion, T. Nakata, S. Suzuki, and H. Liu, Review of biomimetic approaches for drones, *Drones* [online], vol. 6, no. 11 2022, 2022, ISSN: 2504-446X. DOI: [10.3390/drones6110320](https://doi.org/10.3390/drones6110320). available from: <https://www.mdpi.com/2504-446X/6/11/320>.
- [6] E. Ajanic, M. Feroskhan, V. Wüest, and D. Floreano, Sharp turning maneuvers with avian-inspired wing and tail morphing, *Communications Engineering* [online], vol. 1, no. 1 2022,

p. 34, 2022, ISSN: 2731-3395. DOI: 10 . 1038 / s44172 - 022 - 00035 - 2. available from: <https://doi.org/10.1038/s44172-022-00035-2>.

- [7] E. Ajanic, M. Feroskhan, S. Mintchev, F. Noca, and D. Floreano, Bioinspired wing and tail morphing extends drone flight capabilities, *Science Robotics*, vol. 5, no. 47 2020, eabc2897, 2020.
- [8] M. M. Groves-Raines, S. A. Araujo-Estrada, A. Mohamed, S. Watkins, and S. P. Windsor, “Wind tunnel testing of an avian-inspired morphing wing with distributed pressure sensing,” in *2022 International Conference on Unmanned Aircraft Systems (ICUAS)*, 2022, pp. 290–299. DOI: 10 . 1109 / ICUAS54217 . 2022 . 9836045.
- [9] E. Torenbeek, An introduction to wing design, in *Synthesis of Subsonic Airplane Design: An introduction to the preliminary design of subsonic general aviation and transport aircraft, with emphasis on layout, aerodynamic design, propulsion and performance*. Dordrecht: Springer Netherlands, 1982, pp. 215–262, ISBN: 978-94-017-3202-4. DOI: 10 . 1007 / 978 - 94 - 017 - 3202 - 4 _ 7. available from: https://doi.org/10.1007/978-94-017-3202-4_7.
- [10] Unmanned air vehicles, in *Small Unmanned Fixed-wing Aircraft Design*. John Wiley Sons, Ltd, 2017, ch. 2, pp. 15–30, ISBN: 9781119406303. DOI: <https://doi.org/10.1002/9781119406303.ch2>. eprint: <https://onlinelibrary.wiley.com/doi/pdf/10.1002/9781119406303.ch2>. available from: <https://onlinelibrary.wiley.com/doi/abs/10.1002/9781119406303.ch2>.
- [11] M. H. Sadraey, *Aircraft design: A systems engineering approach* (Aerospace Series). Chichester: John Wiley and Sons, 2013, ISBN: 9781118352700. DOI: 10 . 1002 / 9781118352700. available from: <http://dx.doi.org/10.1002/9781118352700>.
- [12] A. Mohamed, K. Massey, S. Watkins, and R. Clothier, The attitude control of fixed-wing mavs in turbulent environments, *Progress in Aerospace Sciences* [online], vol. 66 2014, pp. 37–48, 2014, ISSN: 0376-0421. DOI: <https://doi.org/10.1016/j.paerosci.2013.12.003>. available from: <https://www.sciencedirect.com/science/article/pii/S0376042113000912>.

- [13] S. Watkins and G. Vino, “The turbulent wind environment of birds, insects and mavs,” in *15th Australasian fluid mechanics conference*, Citeseer, 2004.
- [14] S. Watkins, A. Mohamed, A. Fisher, R. Clothier, R. Carrese, and D. F. Fletcher, Towards autonomous mav soaring in cities: Cfd simulation,efd measurement and flight trials, *International Journal of Micro Air Vehicles*, vol. 7, no. 4 2015, pp. 441–448, 2015.
- [15] A. Mohamed, S. Watkins, R. Clothier, and M. Abdulrahim, Influence of turbulence on mav roll perturbations, *International Journal of Micro Air Vehicles*, vol. 6, no. 3 2014, pp. 175–190, 2014.
- [16] S. A. Chin DD Matloff LY, Inspiration for wing design: How forelimb specialization enables active flight in modern vertebrates, *J R Soc Interface* [online] Jun. 2017, p. 131, Jun. 2017. DOI: 10.1098/rsif.2017.0240. available from: <https://pubmed.ncbi.nlm.nih.gov/28592663/>.
- [17] E. L. C. Shepard, C. Williamson, and S. P. Windsor, Fine-scale flight strategies of gulls in urban airflows indicate risk and reward in city living, *Philosophical Transactions of the Royal Society B: Biological Sciences* [online], vol. 371, no. 1704 2016, p. 20150394, 2016. DOI: 10.1098/rstb.2015.0394. eprint: <https://royalsocietypublishing.org/doi/pdf/10.1098/rstb.2015.0394>. available from: <https://royalsocietypublishing.org/doi/abs/10.1098/rstb.2015.0394>.
- [18] A. Hedenström and M. Rosén, Predator versus prey: on aerial hunting and escape strategies in birds, *Behavioral Ecology* [online], vol. 12, no. 2 Mar. 2001, pp. 150–156, Mar. 2001, ISSN: 1045-2249. DOI: 10.1093/beheco/12.2.150. eprint: <https://academic.oup.com/beheco/article-pdf/12/2/150/9742062/120150.pdf>. available from: <https://doi.org/10.1093/beheco/12.2.150>.
- [19] D. Lentink, U. K. Müller, E. J. Stamhuis, *et al.*, How swifts control their glide performance with morphing wings, *Nature* [online], vol. 446, no. 7139 2007, pp. 1082–1085, 2007, ISSN: 1476-4687. DOI: 10.1038/nature05733. available from: <https://doi.org/10.1038/nature05733>.

- [20] A. L. THOMAS and G. K. TAYLOR, Animal flight dynamics i. stability in gliding flight, *Journal of Theoretical Biology* [online], vol. 212, no. 3 2001, pp. 399–424, 2001, ISSN: 0022-5193. DOI: <https://doi.org/10.1006/jtbi.2001.2387>. available from: <https://www.sciencedirect.com/science/article/pii/S0022519301923872>.
- [21] A. K. Stowers, “Avian inspired morphing wings,” English, Copyright - Database copyright ProQuest LLC; ProQuest does not claim copyright in the individual underlying works; Last updated - 2023-03-07, Ph.D. dissertation, 2017, p. 157, ISBN: 9798698507833. available from: <https://bris.idm.oclc.org/login?url=https://www.proquest.com/dissertations-theses/avian-inspired-morphing-wings/docview/2501934048/se-2>.
- [22] C. Harvey, V. B. Baliga, J. C. M. Wong, D. L. Altshuler, and D. J. Inman, Birds can transition between stable and unstable states via wing morphing, *Nature* [online], vol. 603, no. 7902 2022, pp. 648–653, 2022, ISSN: 1476-4687. DOI: 10.1038/s41586-022-04477-8. available from: <https://doi.org/10.1038/s41586-022-04477-8>.
- [23] J. A. Cheney, J. P. J. Stevenson, N. E. Durston, *et al.*, Raptor wing morphing with flight speed, *Journal of The Royal Society Interface* [online], vol. 18, no. 180 2021, p. 20210349, 2021. DOI: 10.1098/rsif.2021.0349. eprint: <https://royalsocietypublishing.org/doi/pdf/10.1098/rsif.2021.0349>. available from: <https://royalsocietypublishing.org/abs/10.1098/rsif.2021.0349>.
- [24] C. Greatwood, A. Waldock, and T. Richardson, Perched landing manoeuvres with a variable sweep wing uav, *Aerospace Science and Technology* [online], vol. 71 2017, pp. 510–520, 2017, ISSN: 1270-9638. DOI: <https://doi.org/10.1016/j.ast.2017.09.034>. available from: <https://www.sciencedirect.com/science/article/pii/S1270963816311889>.
- [25] E. Chang, L. Y. Matloff, A. K. Stowers, and D. Lentink, Soft biohybrid morphing wings with feathers underactuated by wrist and finger motion, *Science Robotics* [online], vol. 5, no. 38 2020, eaay1246, 2020. DOI: 10.1126/scirobotics.aay1246. eprint: <https://www.science.org/doi/pdf/10.1126/scirobotics.aay1246>. available from: <https://www.science.org/doi/abs/10.1126/scirobotics.aay1246>.

- [26] B. N. Pamadi, *Performance, stability, dynamics, and control of airplanes*. Aiaa, 2004.
- [27] C. Harvey, V. B. Baliga, C. D. Goates, D. F. Hunsaker, and D. J. Inman, Gull-inspired joint-driven wing morphing allows adaptive longitudinal flight control, *Journal of The Royal Society Interface* [online], vol. 18, no. 179 2021, p. 20210132, 2021. DOI: 10.1098/rsif.2021.0132. eprint: <https://royalsocietypublishing.org/doi/pdf/10.1098/rsif.2021.0132>. available from: <https://royalsocietypublishing.org/doi/abs/10.1098/rsif.2021.0132>.
- [28] J. A. Jr., *The Airplane: A History of Its Technology*, American Instituteof Aeronautics Astronautics. American Instituteof Aeronautics Astronautics, , 2002,
- [29] D. F. Hunsaker, Z. S. Montgomery, and J. J. Joo, Analytic and computational analysis of wing twist to minimize induced drag during roll, *Proceedings of the Institution of Mechanical Engineers, Part G: Journal of Aerospace Engineering* [online], vol. 234, no. 3 2020, pp. 788–803, 2020. DOI: 10.1177/0954410019886939. eprint: <https://doi.org/10.1177/0954410019886939>. available from: <https://doi.org/10.1177/0954410019886939>.
- [30] J. Young, “Flight control and performance estimation of wild free flying birds and implications for small-unmanned air vehicles,” Ph.D. dissertation, Aerospace Engineering, University of Bristol, Jun. 2023. available from: https://research-information.bris.ac.uk/ws/portalfiles/portal/369713980/Final_Copy_2023_03_24_Young_J_J_PhD.pdf.
- [31] E. Ajanic, “Wing and tail morphing in birds and drones,” Ph.D. dissertation, IGM, Lausanne, 2023, p. 130. DOI: <https://doi.org/10.5075/epfl-thesis-9574>. available from: <http://infoscience.epfl.ch/record/300545>.
- [32] L. Y. Matloff, E. Chang, T. J. Feo, *et al.*, How flight feathers stick together to form a continuous morphing wing, *Science* [online], vol. 367, no. 6475 2020, pp. 293–297, 2020. DOI: 10.1126/science.aaz3358. eprint: <https://www.science.org/doi/pdf/10.1126/science.aaz3358>. available from: <https://www.science.org/doi/abs/10.1126/science.aaz3358>.

- [33] Z. (Hui, Y. (Zhang, and G. (Chen, Tip-vortex flow characteristics investigation of a novel bird-like morphing discrete wing structure, *Physics of Fluids* [online], vol. 32, no. 3 2020, p. 035112, 2020. DOI: 10.1063/1.5144432. eprint: <https://doi.org/10.1063/1.5144432>. available from: <https://doi.org/10.1063/1.5144432>.
- [34] M. V. Cook, Chapter 3 - static equilibrium and trim, in *Flight Dynamics Principles (Third Edition)*, M. V. Cook, Ed., Third Edition, Butterworth-Heinemann, 2013, pp. 33–71, ISBN: 978-0-08-098242-7. DOI: <https://doi.org/10.1016/B978-0-08-098242-7.00003-1>. available from: <https://www.sciencedirect.com/science/article/pii/B9780080982427000031>.
- [35] *Xflr5, analysis of foils and wings operating at low reynolds numbers*. Purdue University, Oct. 2009. available from: [https://engineering.purdue.edu/~aerodyn/AE333/FALL10/HOMEWORKS/HW13/XFLR5_v6.01_Beta_Win32\(2\)/Release/Guidelines.pdf](https://engineering.purdue.edu/~aerodyn/AE333/FALL10/HOMEWORKS/HW13/XFLR5_v6.01_Beta_Win32(2)/Release/Guidelines.pdf).
- [36] F. Healy, R. Cheung, D. Rezgui, and J. Cooper, “Experimental analysis of the behaviour of flared folding wingtips with sideslip angle,” English, 19th International Forum on Aeroelasticity and Structural Dynamics, IFASD 2022, IFASD ; Conference date: 13-06-2022 Through 17-06-2022, Jun. 2022.
- [37] H. F., “Overview and flow survey of the 7 by 5 foot wind tunnelat the university of bristol,” Ph.D. dissertation, Aerospace Engineering, 2023.